Inhibition of striatonigral autophagy as a link between cannabinoid intoxication and impairment of motor coordination

Cristina Blázquez, Andrea Ruiz-Calvo, Raquel Bajo-Grañeras, Jérôme Baufreton, Eva Resel, Marjorie Varilh, Antonio Pagano Zottola, Yamuna Mariani, Astrid Cannich, José Rodríguez-Navarro, et al.

▶ **To cite this version:**

Cristina Blázquez, Andrea Ruiz-Calvo, Raquel Bajo-Grañeras, Jérôme Baufreton, Eva Resel, et al.. Inhibition of striatonigral autophagy as a link between cannabinoid intoxication and impairment of motor coordination. eLife, 2020, 9, 10.7554/eLife.56811 . hal-02988865

HAL Id: hal-02988865
https://hal.science/hal-02988865

Submitted on 6 Nov 2020

HAL is a multi-disciplinary open access archive for the deposit and dissemination of scientific research documents, whether they are published or not. The documents may come from teaching and research institutions in France or abroad, or from public or private research centers.

L'archive ouverte pluridisciplinaire **HAL**, est destinée au dépôt et à la diffusion de documents scientifiques de niveau recherche, publiés ou non, émanant des établissements d'enseignement et de recherche français ou étrangers, des laboratoires publics ou privés.

RESEARCH ARTICLE

Inhibition of striatonigral autophagy as a link between cannabinoid intoxication and impairment of motor coordination

Cristina Blázquez[1,2], Andrea Ruiz-Calvo[1,2], Raquel Bajo-Grañeras[1,2], Jérôme M Baufreton[3], Eva Resel[1,2], Marjorie Varilh[4], Antonio C Pagano Zottola[4], Yamuna Mariani[4], Astrid Cannich[4], José A Rodríguez-Navarro[2], Giovanni Marsicano[4], Ismael Galve-Roperh[1,2], Luigi Bellocchio[4]*, Manuel Guzmán[1,2]*

[1]Centro de Investigación Biomédica en Red sobre Enfermedades Neurodegenerativas (CIBERNED), Instituto Universitario de Investigación Neuroquímica (IUIN) and Department of Biochemistry and Molecular Biology, Complutense University, Madrid, Spain; [2]Instituto Ramón y Cajal de Investigación Sanitaria (IRYCIS), Madrid, Spain; [3]Centre National de la Recherche Scientifique (CNRS) and University of Bordeaux, Institut des Maladies Neurodégénératives, Bordeaux, France; [4]Institut National de la Santé et de la Recherche Médicale (INSERM) and University of Bordeaux, NeuroCentre Magendie, Physiopathologie de la Plasticité Neuronale, Bordeaux, France

Abstract The use of cannabis is rapidly expanding worldwide. Thus, innovative studies aimed to identify, understand and potentially reduce cannabis-evoked harms are warranted. Here, we found that Δ^9-tetrahydrocannabinol, the psychoactive ingredient of cannabis, disrupts autophagy selectively in the striatum, a brain area that controls motor behavior, both in vitro and in vivo. Boosting autophagy, either pharmacologically (with temsirolimus) or by dietary intervention (with trehalose), rescued the Δ^9-tetrahydrocannabinol-induced impairment of motor coordination in mice. The combination of conditional knockout mouse models and viral vector-mediated autophagy-modulating strategies in vivo showed that cannabinoid CB_1 receptors located on neurons belonging to the direct (striatonigral) pathway are required for the motor-impairing activity of Δ^9-tetrahydrocannabinol by inhibiting local autophagy. Taken together, these findings identify inhibition of autophagy as an unprecedented mechanistic link between cannabinoids and motor performance, and suggest that activators of autophagy might be considered as potential therapeutic tools to treat specific cannabinoid-evoked behavioral alterations.

***For correspondence:**
luigi.bellocchio@inserm.fr (LB);
mguzman@quim.ucm.es (MG)

Competing interests: The authors declare that no competing interests exist.

Funding: See page 19

Received: 10 March 2020
Accepted: 14 July 2020
Published: 10 August 2020

Reviewing editor: Joseph F Cheer, University of Maryland School of Medicine, United States

© Copyright Blázquez et al. This article is distributed under the terms of the Creative Commons Attribution License, which permits unrestricted use and redistribution provided that the original author and source are credited.

Introduction

Cannabis is one of the most common drugs of abuse in the world (***Alpár et al., 2016***; ***Englund et al., 2017***; ***Volkow et al., 2014***). Consequently, its major intoxicating constituent, the cannabinoid Δ^9-tetrahydrocannabinol (THC), is the third most popular recreational addictive chemical following ethanol and nicotine. Of note, several states in the USA, as well as a few countries in the world, have legalized the recreational use of cannabis. Cannabis preparations have also been used in medicine for millennia, and nowadays there is a vigorous renaissance in the study and application of their therapeutic effects (***Pertwee, 2012***). In this context, THC and other cannabinoids are already approved by various regulatory agencies, including the Food and Drug Administration (FDA), the European Medicines Agency and Health Canada, as anti-emetic, anti-cachexic, analgesic

and anti-spastic compounds (**Hill, 2015**; **Whiting et al., 2015**). Moreover, medical-grade cannabis dispensation programs have been implemented in about half of the states in the USA and in a growing number of countries globally. However, cannabis use is associated to several undesired and possibly dangerous side effects, so it is crucial that innovative procedures aimed to understand and potentially reduce cannabis-evoked harms are explored (**Alpár et al., 2016**; **Englund et al., 2017**; **Volkow et al., 2014**).

THC exerts its biological effects mainly by activating cannabinoid CB_1 receptor, one of the most abundant metabotropic receptors in the mammalian central nervous system (**Katona and Freund, 2008**; **Pertwee et al., 2010**). This receptor is particularly expressed in discrete brain areas involved in the control of learning and memory (cortex, hippocampus), motor behavior (striatum, cerebellum), emotions (amygdala), and autonomic and endocrine functions (hypothalamus, pons, medulla), therefore participating in the control of a wide plethora of biological processes (**Katona and Freund, 2008**; **Mechoulam and Parker, 2013**). A family of retrograde lipid messengers, the endocannabinoids, biologically engages the CB_1 receptor, mediating a feedback mechanism aimed to prevent excessive neuronal activity and, thereby, tuning the functionality and plasticity of many synapses (**Castillo et al., 2012**; **Piomelli, 2003**). Recent evidence suggests that the CB_1 receptor can control autophagy, a highly conserved and pleiotropic process of cellular 'self-digestion' in which cytoplasmic materials are sequestered into double-membrane vesicles called autophagosomes, and subsequently delivered to lysosomes for degradation or recycling (**Costa et al., 2016**; **Hiebel and Behl, 2015**). Autophagy is an essential mechanism of cellular quality control, and the knowledge on its biological functions in the brain and other organs is rapidly increasing (**Menzies et al., 2017**; **Ohsumi, 2014**). Strikingly, in some cell-culture settings cannabinoids via the CB_1 receptor enhance autophagy (**Koay et al., 2014**; **Salazar et al., 2009**), while in others they inhibit autophagy (**Hiebel et al., 2014**; **Piyanova et al., 2013**). Moreover, it is not known yet whether the CB_1 receptor controls autophagy in the brain in vivo, and, eventually, what the functional consequences of this potential CB_1 receptor/autophagy connection could be. Here, we show that THC inhibits autophagy selectively in the mouse striatum, and that this process participates in the THC-induced impairment of motor coordination. Moreover, administration of clinically safe autophagy activators to mice prevents the dyscoordinating effect of THC. These findings unveil an unprecedented link between cannabinoids, autophagy and motor performance, and provide preclinical evidence for the design of potential new therapeutic strategies aimed at treating specific cannabinoid-induced behavioral alterations.

Results

THC impairs striatal autophagy both in vivo and in vitro

To study the effect of THC on autophagy in the brain we first treated wild-type mice with a single i.p. injection of the drug at 10 mg/kg or its vehicle. After 4 hr, we evaluated the status of key autophagy protein markers. This dose and time window allows assessing persistent and pharmacologically tractable behavioral actions of THC administration, as previously reported (**Metna-Laurent et al., 2017**; **Puighermanal et al., 2013**). We analyzed the expression pattern of microtubule-associated light chain three protein (LC3), the most widely used marker of autophagic vesicles (autophagosomes) (**Mizushima et al., 2011**; **Ohsumi, 2014**), in representative brain structures. Upon induction of autophagy, LC3 is converted from a soluble, non-lipidated form (LC3-I) to an aggregated, phosphatidylethanolamine-conjugated form (LC3-II), thereby becoming recruited to autophagosomal membranes (**Mizushima et al., 2011**). THC increased LC3-II levels in the striatum, either when referred to LC3-I (THC vs. vehicle, $t = 4.680$; df = 10; p=0.0009) or to β-actin (THC vs. vehicle, $t = 4.331$; df = 10; p=0.0015) as control, but not in other representative brain regions as the cortex, the hippocampus and the cerebellum (**Figure 1A**). An elevation of LC3-II levels, however, may indicate either that THC increases autophagosome generation (and so increases autophagic flux) or that THC decreases autophagosome clearance (and so decreases autophagic flux) (**Mizushima et al., 2011**; **Ohsumi, 2014**). To discern between these two possibilities, we measured the levels of p62 (sequestosome 1), a pivotal adaptor protein that carries cargo proteins to the autophagosome, being subsequently degraded upon fusion of the autophagosome to the lysosome (autophagolysosome or autolysosome) (**Katsuragi et al., 2015**; **Mizushima et al., 2011**). Hence, an

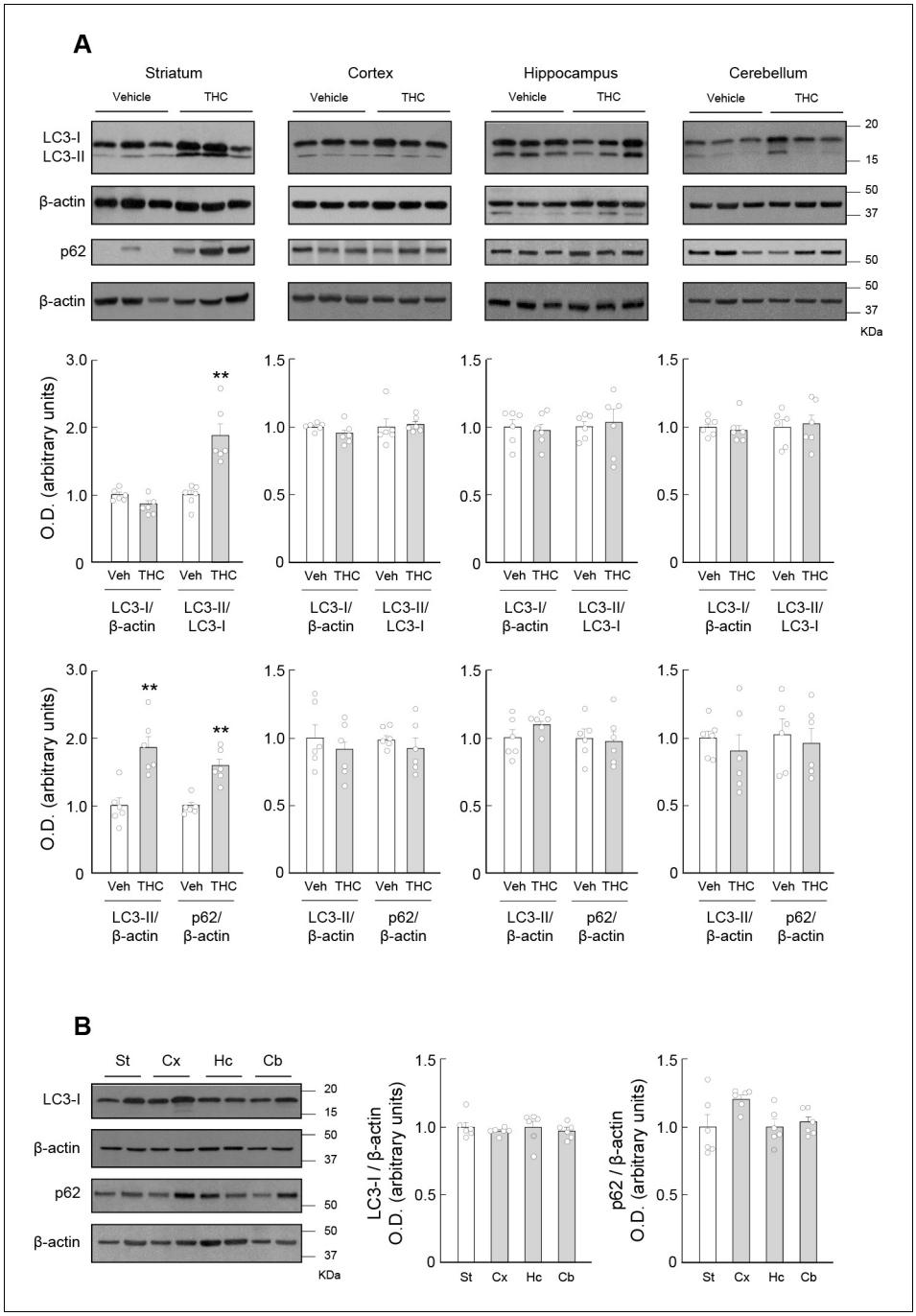

Figure 1. THC impairs autophagy in the mouse striatum. Wild-type C57BL/6N mice were treated with THC (10 mg/kg as a single i.p. injection) or its vehicle. Four hours later, the striatum (St), cortex (Cx), hippocampus (Hc) and cerebellum (Cb) were dissected for Western blot analysis. (**A**) Effect of THC on autophagy markers in the different brain regions. (**B**) Relative levels of LC3-I and p62 in the different brain regions from vehicle-treated animals. In both panels, representative blots of each condition, together with optical density values relative to those of the respective loading controls, are shown (n = 6 animals per group). Blots were cropped for clarity. Electrophoretic migration of molecular weight markers is depicted on the right-hand side of each blot. **p<0.01 from vehicle-treated group by unpaired Student t-test. Raw numerical data and further statistical details are shown in ***Figure 1—source data 1***.

The online version of this article includes the following source data for figure 1:

Source data 1. Source data for THC impairs autophagy in the mouse striatum.

increase of LC3-II together with a decrease of p62 usually denotes an active clearance of autophagosomes (and so an increased autophagic flux), while a simultaneous elevation of LC3-II and p62 usually defines an impaired clearance of autophagosomes (and so a decreased autophagic flux) (**Katsuragi et al., 2015**; **Mizushima et al., 2011**). THC induced an accumulation of p62 in the striatum (THC vs. vehicle, t = 5.303; df = 10; p=0.0003), but not in the other brain regions tested (**Figure 1A**), thus indicating that THC impairs the execution of autophagy and that this process occurs selectively in the striatum. Of note, the levels of LC3-I and p62 were not significantly different in the striatum than in the cortex, hippocampus or cerebellum from vehicle-treated mice (**Figure 1B**), suggesting that the selective impact of THC on striatal autophagy does not rely on the basal expression of those two key autophagy proteins but on additional, hitherto unknown molecular factors.

To support a direct action of THC on the striatum, we prepared primary cultures of mouse striatal neurons and treated them with THC (0.75 µM). The synthetic THC analogue HU-210 (10 nM) was used as a further tool to proof pharmacological specificity. The two cannabinoid drugs increased LC3-II levels, as determined by immunofluorescence (aggregated-LC3 *puncta*), in both the total intracellular compartment ($F_{(2,28)}$ = 39.48; THC vs. vehicle, p=0.0004; HU-210 vs. vehicle, p<0.0001) and the lysosomal compartment, as identified by the lysosomal marker LAMP1 ($F_{(2,28)}$ = 22.43; THC vs. vehicle, p<0.0001, HU-210 vs. vehicle: p<0.0001) (**Figure 2A**). Concertedly, they also enhanced p62 levels ($F_{(2,30)}$ = 38.81; THC vs. vehicle, p=0.0130; HU-210 vs. vehicle, p=0.0335) (**Figure 2B**). We next evaluated the effect of the direct inhibition of lysosomal degradation. Upon this downstream blockade of autophagic flux, an autophagy-stimulating compound conceivably induces a further accumulation of autophagosomal markers (LC3-II and p62), while an autophagy-inhibiting compound is not expected to raise those markers further (**Mizushima et al., 2011**). We thus treated striatal neurons with two types of lysosomal inhibitors, specifically the lysosomotropic drug hydroxychloroquine or the lysosomal-protease inhibitors E64d and pepstatin A. As expected, these lysosome-blocking drugs induced per se an accumulation of LC3-II (total LC3-II: $F_{(2,28)}$ = 39.48; hidroxychloroquine vs. vehicle, p<0.0001; E64d/pepstatin A vs. vehicle, p=0.0024. LC3-II/LAMP1: $F_{(2,28)}$ = 22.43; hidroxychloroquine vs. vehicle: p<0.0001; E64d/pepstatin A vs. vehicle: p=0.0002) (**Figure 2A**) and p62 ($F_{(2,30)}$ = 38.81; hidroxychloroquine vs. vehicle, p=0.0001; E64d/pepstatin A vs. vehicle, p<0.0001) (**Figure 2B**). Of note, cannabinoids did not significantly heighten those pre-augmented levels of LC3-II (**Figure 2A**) and p62 (**Figure 2B**).

Taken together, these data support that cannabinoids inhibit autophagic flux in striatal neurons both in vivo and in vitro.

Temsirolimus prevents the THC-induced impairment of striatal autophagy and motor coordination in vivo

THC and other cannabinoids modulate various intracellular signalling pathways in the brain by engaging CB_1 receptors (**Castillo et al., 2012**; **Pertwee et al., 2010**). One of the most relevant CB_1 receptor-evoked actions is the activation of the phosphatidylinositol-3-kinase/Akt/mammalian target of rapamycin complex 1 (mTORC1) pathway (**Blázquez et al., 2015**; **Gómez del Pulgar et al., 2000**; **Ozaita et al., 2007**; **Puighermanal et al., 2009**). The serine/threonine kinase mTOR, the catalytic component of mTORC1, is critically involved in the control of neural plasticity through the regulation of protein synthesis and other basic cellular functions (**Bockaert and Marin, 2015**; **Lipton and Sahin, 2014**). Of note, mTORC1 is also the most relevant signaling platform that exerts a negative control on autophagy by phosphorylating UNC-51-like kinase 1 (ULK1), and so inhibiting autophagosome formation (**Dunlop and Tee, 2014**; **Saxton and Sabatini, 2017**). However, it is not known whether a cannabinoid-evoked activation of the mTORC1 pathway would be linked to an inhibition of autophagy, and, especially, what the biological consequences of this process could be.

To address this question, we made use of temsirolimus, an FDA-approved rapamycin analogue that selectively blocks mTOR within mTORC1, thereby disinhibiting autophagy (**Dunlop and Tee, 2014**). Mice were treated with temsirolimus (1 mg/kg, i.p.) or its vehicle, and, 20 min later, with THC (10 mg/kg, i.p.) or its vehicle. As THC inhibited autophagy selectively in the striatum, animals were subjected to tests of motor behavior, an archetypical process that - together with, for example, cognition, affection and reward - is controlled by the striatum and is impacted by cannabinoids in both laboratory animals and humans (**Koketsu et al., 2008**; **Kreitzer, 2009**; **Lovinger, 2010**). Four hours after injection, THC impaired motor coordination, as determined by the RotaRod test, and

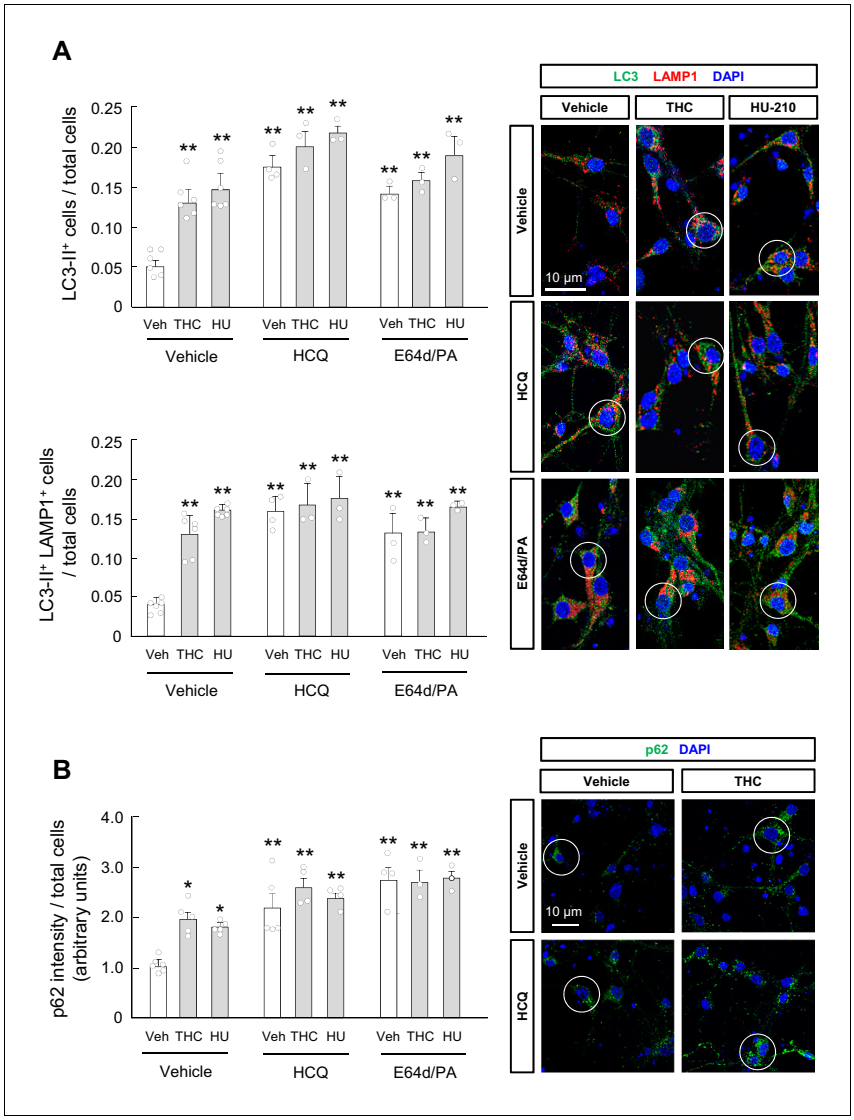

Figure 2. THC impairs autophagy in primary striatal neurons. Primary striatal neurons from C57BL/6N mice were exposed for 24 hr to THC (0.75 µM) or HU-210 (10 nM), alone or in combination with hydroxychloroquine (0.1 mM), E64d (0.1 µM) and/or pepstatin A (10 ng/ml), or their vehicles. (**A**) LC3-II immunoreactivity (number of cells with three or more LC3-positive dots relative to total cells; *upper panel*) and LC3-II/LAMP1 immunoreactivity (number of LAMP1-positive cells with three or more LC3 dots relative to total cells; *lower panel*). Representative images with encircled examples of double-positive cells are shown (n = 3–6 independent cell preparations per condition). (**B**) p62 immunoreactivity (p62 fluorescence intensity relative to total cells). Representative images of selected experimental conditions with encircled examples of high-intensity cells are shown (n = 3–6 independent cell preparations per condition). *p<0.05, **p<0.01 from vehicle-treated group by two-way ANOVA with Tukey's multiple comparisons test. Raw numerical data and further statistical details are shown in ***Figure 2—source data 1***.

The online version of this article includes the following source data for figure 2:

Source data 1. Source data for THC impairs autophagy in primary striatal neurons.

temsirolimus, under conditions that did not influence behavior by itself, rescued the effect of THC ($F_{(3,30)}$ = 6.635; THC vs. vehicle, p=0.0016; temsirolimus + THC vs. THC, p=0.0096) (***Figure 3A***). In contrast, the inhibitory action of THC on general locomotor activity, as determined by various parameters in the open field test (THC vs. vehicle, ambulation: $F_{(3,24)}$ = 24.14; p=0.0002; activity: $F_{(3,24)}$ = 10.67; p=0.0241; resting time: $F_{(3,24)}$ = 13.89; p=0.0067; fast movements: $F_{(3,24)}$ = 14.15; p=0.0002; stereotypic movements: $F_{(3,24)}$ = 8.240; p=0.0137), was not significantly affected by

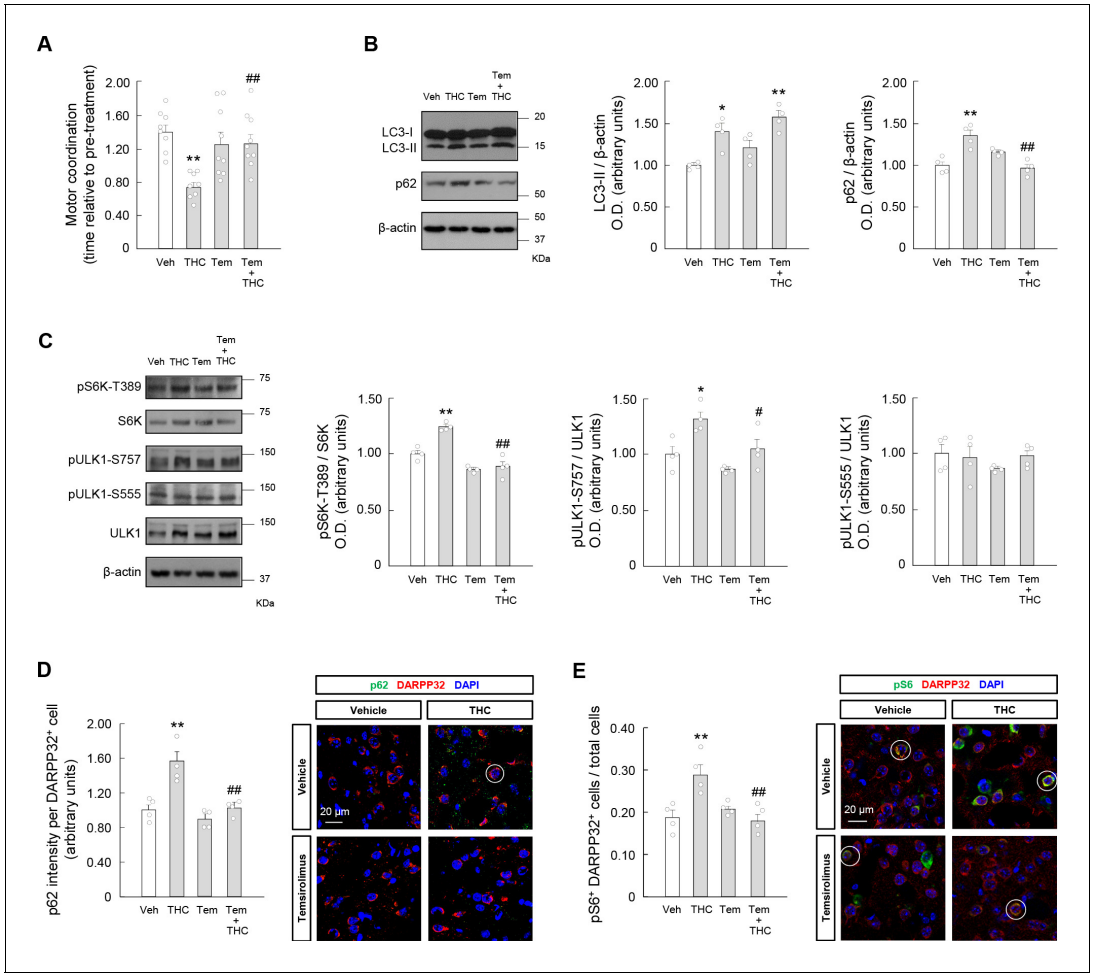

Figure 3. Temsirolimus prevents the THC-induced impairment of striatal autophagy and motor coordination in vivo. Wild- type C57BL/6N mice were treated with temsirolimus (1 mg/kg as a single i.p. injection) or its vehicle for 20 min, and, subsequently, with THC (10 mg/kg as a single i.p. injection) or its vehicle for 4 hr. (**A**) Motor coordination (RotaRod test, time to fall relative to pre-treatment; *n* = 8–9 animals per group). (**B, C**) Western blot analysis of autophagy markers (*panel B*) and mTORC1 signaling pathway markers (*panel C*) in the striatum. Representative blots of each condition, together with optical density values relative to those of loading controls, are shown (*n* = 4 animals per group). Blots were cropped for clarity. Electrophoretic migration of molecular weight markers is depicted on the right-hand side of each blot. (**D, E**) Immunofluorescence analysis of p62 (p62 fluorescence intensity per DARPP32-positive cell; *panel D*) and phosphorylated ribosomal protein S6 (phospho-S6/DARPP32 double-positive cells relative to total cells; *panel E*) in the dorsal striatum (*n* = 4 animals per group). Representative images with encircled examples of a high-intensity cell (*panel D*) or double-positive cells (*panel E*) are shown. *p<0.05, **p<0.01 from vehicle-treated group, or #p<0.05, ##p<0.01 from THC-treated group, by one-way ANOVA with Tukey's multiple comparisons test. Raw numerical data and further statistical details are shown in ***Figure 3—source data 1***.
The online version of this article includes the following source data and figure supplement(s) for figure 3:

Source data 1. Source data for Temsirolimus prevents the THC-induced impairment of striatal autophagy and motor coordination in vivo.
Figure supplement 1. Temsirolimus does not rescue THC-induced hypolocomotion.

temsirolimus (***Figure 3—figure supplement 1***; ***Puighermanal et al., 2013***). This supports the idea that the THC-induced activation of the mTORC1 pathway selectively affects the coordination component of motor behavior. Under these experimental conditions, western blot analysis of mouse striata supported that THC concomitantly inhibited autophagy, as determined by the simultaneous accumulation of LC3-II (THC vs. vehicle, $F_{(3,12)}$ = 10.77; p=0.0119) and p62 (THC vs. vehicle, $F_{(3,12)}$ = 12.29; p=0.0017) (***Figure 3B***), and activated the mTORC1 pathway, as determined by an enhanced phosphorylation of the mTORC1-dependent sites in two of its main substrates, namely T389 in 70 kDa ribosomal protein S6 kinase (S6K) (THC vs. vehicle, $F_{(3,12)}$ = 28.70; p=0.0009), and S757 in ULK1 (THC vs. vehicle, $F_{(3,12)}$ = 8.506; p=0.0214) (***Figure 3C***). Of note, temsirolimus rescued these

cannabinoid-evoked effects on p62 (temsirolimus + THC vs. THC, $F_{(3,12)}$ = 12.29; p=0.0008) (***Figure 3B***) and the mTORC1 pathway markers (pS6K-T389: temsirolimus + THC vs. THC, $F_{(3,12)}$ = 28.70; p<0.0001. pULK1-S757: temsirolimus + THC vs. THC, $F_{(3,12)}$ = 8.506; p=0.0470) (***Figure 3C***). Similar data were obtained by immunofluorescence analysis of p62 levels ($F_{(3,12)}$ = 16.80; THC vs. vehicle, p=0.0009; temsirolimus + THC vs. THC, p=0.0011) (***Figure 3D***), and of the phosphorylation state of the mTORC1/S6K downstream effector ribosomal protein S6 at two target residues (S235/S236) ($F_{(3,12)}$ = 8.34; THC vs. vehicle, p=0.0052; temsirolimus + THC vs. THC, p=0.0047) (***Figure 3E***), in striatal medium spiny neurons (MSNs), as identified by their standard marker dopamine- and cAMP-regulated phosphoprotein of 32 kDa (DARPP32). As a control, we found that the phosphorylation state of the main AMP-activated protein kinase (AMPK)-dependent site in ULK1, namely S555, was not significantly affected by THC and/or temsirolimus (***Figure 3C***). We were unable to immunodetect significant amounts of LC3 *puncta* in brain sections, which is usually ascribed to the rapid autophagic turnover and very high abundance of LC3-I over LC3-II occurring in living brain tissue (***McMahon et al., 2012***; ***Mizushima et al., 2004***; ***Sarkar et al., 2014***; ***Yang et al., 2011***).

Taken together, these findings suggest that an inhibition of autophagy participates in the motor-dyscoordinating action of THC.

Trehalose prevents the THC-induced impairment of striatal autophagy and motor coordination in vivo

As a second approach to manipulate autophagy in vivo, we used the natural disaccharide trehalose, which directly stimulates autophagic flux (***Emanuele, 2014***; ***Sarkar et al., 2007***). Mice were given trehalose (10 g/L in drinking water) or plain water for 24 hr, and, subsequently, were treated with THC (10 mg/kg, i.p.) or vehicle. Experimental measures were performed 4 hr after acute THC injection. Trehalose, under conditions that did not affect behavior by itself, rescued the THC-evoked impairment of motor coordination ($F_{(3,45)}$ = 3.858; THC vs. vehicle, p=0.0321; trehalose + THC vs. THC, p=0.0358) (***Figure 4A***). As shown above for temsirolimus, the inhibitory action of THC on general locomotor activity, as determined by various parameters in the open field test (THC vs. vehicle, ambulation: $F_{(3,27)}$ = 7.548; p=0.0402; activity: $F_{(3,27)}$ = 8.536; p=0.0134; resting time: $F_{(3,27)}$ = 7.420; p=0.0154; fast movements: $F_{(3,27)}$ = 8.496; p=0.0356; stereotypic movements: $F_{(3,27)}$ = 9.173; p=0.0032), was not significantly affected by trehalose (***Figure 4—figure supplement 1***). Western blot analysis of mouse striata indicated that trehalose reduced the THC-induced accumulation of striatal p62 ($F_{(3,12)}$ = 23.66; THC vs. vehicle, p=0.0017; trehalose + THC vs. THC, p<0.0001) (***Figure 4B***). Trehalose per se did not significantly affect mTORC1 activity markers, but mitigated the THC-evoked stimulation of the pathway (pS6K-T389: $F_{(3,12)}$ = 5.410; THC vs. vehicle, p=0.0388; trehalose + THC vs. THC, p=0.1944. pULK1-S757: $F_{(3,12)}$ = 12.03; THC vs. vehicle, p=0.0032; trehalose + THC vs. THC, p=0.0074) (***Figure 4C***). ULK1-S555 phosphorylation was not significantly affected by THC and/or trehalose (***Figure 4C***). These western blot data were corroborated by immunofluorescence analysis of p62 levels ($F_{(3,12)}$ = 7.575; THC vs. vehicle, p=0.0075; trehalose + THC vs. THC, p=0.0495) (***Figure 4D***) and protein S6 phosphorylation ($F_{(3,12)}$ = 8.822; THC vs. vehicle, p=0.0040; trehalose + THC vs. THC, p=0.0036) (***Figure 4E***).

Taken together, these findings provide further support to the notion that an inhibition of striatal autophagy participates in the motor-dyscoordinating activity of THC.

Cannabinoid CB_1 receptors located on the direct pathway, but not on cortical projections, are required for the THC-induced impairment of striatal autophagy and motor coordination in vivo

We subsequently studied the neuroanatomical substrate of the observed THC effects. As THC exerts most of its neurobiological effects by activating CB_1 receptors, we first tested the effect of the CB_1 receptor-selective antagonist SR141716 (rimonabant) on the THC-evoked inhibition of motor coordination. Mice were treated with rimonabant (3 mg/kg, i.p.) or vehicle for 20 min, and, subsequently, with THC (10 mg/kg, i.p.) or vehicle. Four hours after injection, THC impaired RotaRod performance, and rimonabant, under conditions that did not influence behavior by itself, abrogated the effect of THC ($F_{(3,16)}$ = 12.86; THC vs. vehicle, p=0.0020; rimonabant + THC vs. THC, p=0.0002) (***Figure 5—figure supplement 1***).

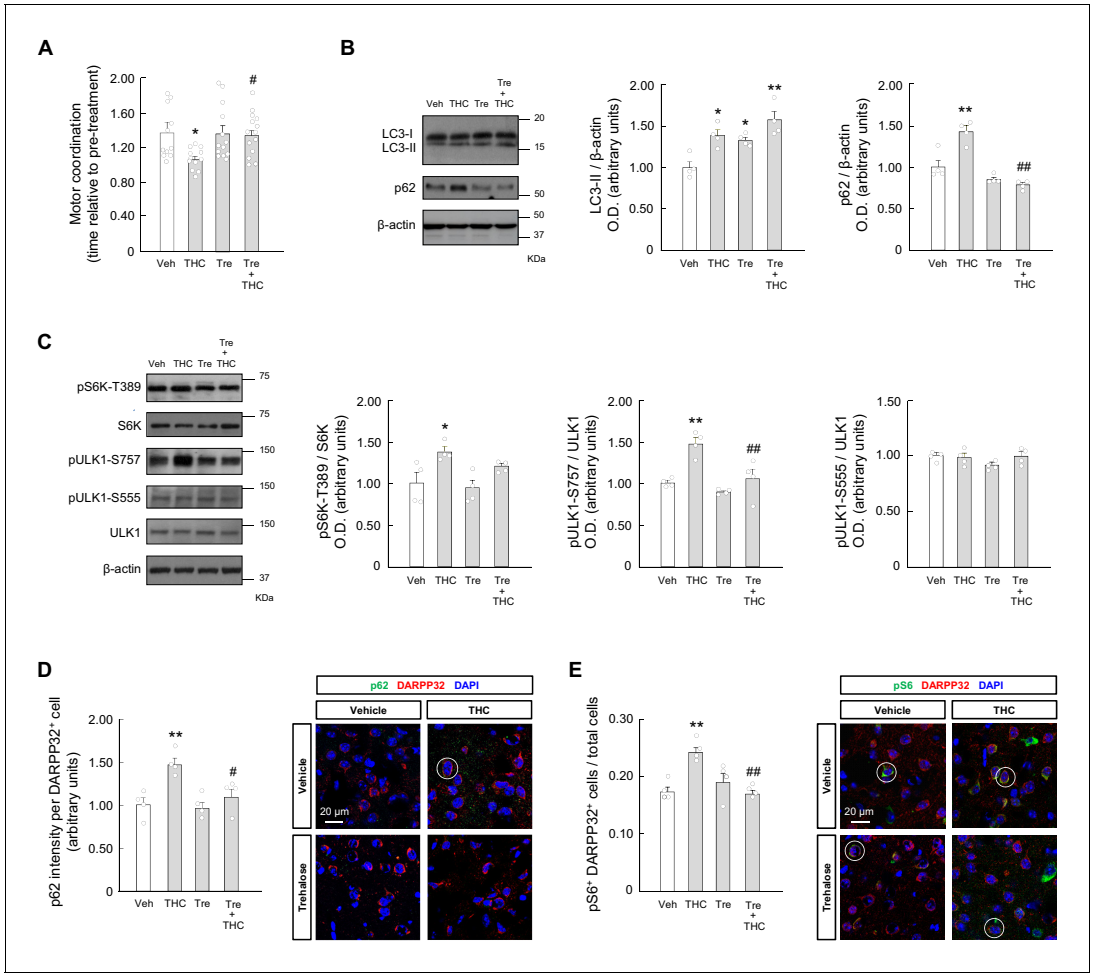

Figure 4. Trehalose prevents the THC-induced impairment of striatal autophagy and motor coordination in vivo. Wild-type C57BL/6N mice were given trehalose (10 g/L) or plain water ad libitum for 24 hr, and, subsequently, were treated with THC (10 mg/kg as a single i.p.injection) or its vehicle for 4 hr. (**A**) Motor coordination (RotaRod test, time to fall relative to pre-treatment; *n* = 11–14 animals per group). (**B, C**) Western blot analysis of autophagy markers (*panel B*) and mTORC1 signaling pathway markers (*panel C*) in the striatum. Representative blots of each condition, together with optical density values relative to those of loading controls, are shown (*n* = 4 animals per group). (**D, E**) Immunofluorescence analysis of p62 (p62 fluorescence intensity per DARPP32-positive cell; *panel D*) and phosphorylated ribosomal protein S6 (phospho-S6/DARPP32 double-positive cells relative to total cells; *panel E*) in the dorsal striatum (*n* = 4 animals per group). Representative images with encircled examples of a high-intensity cell (*panel D*) or double-positive cells (*panel E*) are shown. *p<0.05, **p<0.01 from vehicle-treated group, or $^{\#}$p<0.05, $^{\#\#}$p<0.01 from THC-treated group, by one-way ANOVA with Tukey's multiple comparisons test. Raw numerical data and further statistical details are shown in ***Figure 4—source data 1***.

The online version of this article includes the following source data and figure supplement(s) for figure 4:

Source data 1. Source data for Trehalose prevents the THC-induced impairment of striatal autophagy and motor coordination in vivo.
Figure supplement 1. Trehalose does not rescue THC-induced hypolocomotion.

Striatal MSNs differ in their neurochemical composition and form two major efferent pathways: the direct (striatonigral) pathway, and the indirect (striatopallidal) pathway (***Kreitzer, 2009***). MSNs in the direct pathway (referred to here as D_1R-MSNs) express dopamine D_1 receptor (D_1R), while MSNs in the indirect pathway (referred to here as D_2R-MSNs) express dopamine D_2 receptor (D_2R). It has been reported that *Cnr1*$^{fl/fl}$ mice (referred to here as CB_1R-floxed mice) that had been bred with *Drd1a*^{Cre} mice to inactivate CB_1 receptors selectively in all cells that express D_1R (these mice are referred to here as D_1R-CB_1R KO mice) exhibit a dampened response to the cataleptic effect (but not the overall hypolocomotor effect) of THC (***Monory et al., 2007***). This supports the notion that CB_1 receptors located on D_1R-MSNs control particular aspects of motor behavior. Hence, we evaluated the RotaRod test in D_1R-CB_1R KO mice and their control CB_1R-floxed littermates. Remarkably, the motor-dyscoordinating action of THC (10 mg/kg, i.p.) found in CB_1R-floxed mice was not

evident in D_1R-CB_1R KO animals ($F_{(3,18)}$ = 6.571; CB_1R-floxed-THC vs. CB_1R-floxed-vehicle, p=0.0067; D_1R-CB_1R KO-THC vs. CB_1R-floxed-THC, p=0.0068) (***Figure 5A***). In concert, the simultaneous accumulation of LC3-II and p62 evoked by THC in control mice, as assessed by western blot, was not observed in D_1R-CB_1R KO mice (LC3-II: $F_{(3,12)}$ = 6.981; CB_1R-floxed-THC vs. CB_1R-floxed-vehicle, p=0.0066; D_1R-CB_1R KO-THC vs. CB_1R-floxed-THC, p=0.0122. p62: $F_{(3,12)}$ = 13.36; CB_1R-floxed-THC vs. CB_1R-floxed-vehicle, p=0.0014; D_1R-CB_1R KO-THC vs. CB_1R-floxed-THC, p=0.0005) (***Figure 5B***). The p62 data were confirmed by immunofluorescence analysis ($F_{(3,9)}$ = 14.36; CB_1R-floxed-THC vs. CB_1R-floxed-vehicle, p=0.0038; D_1R-CB_1R KO-THC vs. CB_1R-floxed-THC, p=0.0029) (***Figure 5C***).

By dampening glutamate outflow onto MSNs, CB_1 receptors located on corticostriatal projections are considered a key determinant of striatal activity (***Kreitzer, 2009***; ***Lovinger, 2010***), mediating, specifically, THC-induced hypolocomotion (***Monory et al., 2007***). We therefore evaluated the possible implication of this CB_1 receptor pool in our model. For this purpose, we bred CB_1R-floxed mice with *Neurod6*^{Cre} mice to inactivate CB_1 receptors selectively in all cells that express NeuroD6 (essentially dorsal telencephalic glutamatergic neurons; these mice are referred to here as Glu-CB_1R KO mice) (***Monory et al., 2006***). Administration of THC (10 mg/kg, i.p.) decreased RotaRod performance comparably in Glu-CB_1R KO mice and their control CB_1R-floxed littermates ($F_{(3,12)}$ = 65.18; CB_1R-floxed-THC vs. CB_1R-floxed-vehicle, p<0.0001; Glu-CB_1R KO-THC vs. Glu-CB_1R KO-vehicle, p<0.0001) (***Figure 5D***). Likewise, as assessed by western blot, THC enhanced LC3-II and p62 levels similarly in Glu-CB_1R KO and CB_1R-floxed mice (LC3-II: $F_{(3,12)}$ = 9.471; CB_1R-floxed-THC vs. CB_1R-floxed-vehicle, p=0.0182; Glu-CB_1R KO-THC vs. Glu-CB_1R KO-vehicle, p=0.0107. p62: $F_{(3,12)}$ = 9.462; CB_1R-floxed-THC vs. CB_1R-floxed-vehicle, p=0.0093; Glu-CB_1R KO-THC vs. Glu-CB_1R KO-vehicle, p=0.0168) (***Figure 5E***). The p62 data were confirmed by immunofluorescence analysis ($F_{(3,12)}$ = 11.31; CB_1R-floxed-THC *vs.* CB_1R-floxed-vehicle, p=0.0043; Glu-CB_1R KO-THC *vs.* Glu-CB_1R KO-vehicle, p=0.0108) (***Figure 5F***).

We finally aimed to strengthen the link between the effects of THC on autophagy and motor coordination in D_1R-MSNs. We first treated transgenic mice expressing the tdTomato and EGFP reporter genes under the control of the promoter of the *Drd1a* gene (which encodes D_1R) and the *Drd2* gene (which encodes D_2R), respectively, with THC (10 mg/kg, i.p.) or vehicle. Four hours later, immunofluorescence analysis revealed that the THC-induced activation of the mTORC1 pathway (as determined by protein S6 phosphorylation) occurred selectively in D_1R-MSNs ($F_{(3,15)}$ = 7.387; D_1R-MSN-THC vs. D_1R-MSN-vehicle, p=0.0058; D_2R-MSN-THC vs. D_1R-MSN-THC, p=0.0146) (***Figure 6—figure supplement 1***). Then, we conducted viral vector-enforced protein expression experiments in vivo. We injected stereotactically into the dorsal striatum of D_1R-Cre mice a CAG-DIO rAAV vector carrying a Cre-dependent dominant-negative form of Raptor, one of the essential components of mTORC1 (***Hara et al., 2002***; ***Koketsu et al., 2008***), thus allowing the Cre-driven expression of dominant-negative Raptor in D_1R-MSNs (c-myc-dnRaptor$^+$ cells: D_1R-Cre vs. WT, t = 33.71; df = 6; p<0.0001. pS6$^+$ cells: $F_{(3,9)}$ = 52.52; THC-WT vs. vehicle-WT, p=0.0002; vehicle-D_1R-Cre vs. vehicle-WT, p=0.0205; THC-D_1R-Cre vs. THC-WT, p<0.0001) (***Figure 6A***). Dominant-negative Raptor did not affect RotaRod performance in vehicle-treated animals, but prevented the THC-induced impairment of motor coordination ($F_{(7,28)}$ = 5.309; THC-WT/post-treatment vs. vehicle-WT/post-treatment, p=0.0010; THC-D_1R-Cre/post-treatment vs. THC-WT/post-treatment, p=0.0034) (***Figure 6A***). We next injected stereotactically into the dorsal striatum of D_1R-Cre mice a CAG-DIO rAAV vector encoding p62, thus allowing the Cre-driven expression of p62 in D_1R-MSNs (p62 intensity: D_1R-Cre vs. WT, t = 12.22; df = 6; p<0.0001) (***Figure 6B***). Of note, p62 overexpression per se decreased RotaRod performance in vehicle-treated animals, and this decrease was not additive to that induced by THC administration (10 mg/kg, i.p.) ($F_{(7,28)}$ = 5.641; THC-WT/post-treatment vs. vehicle-WT/post-treatment, p=0.0152; vehicle-D_1R-Cre/pre-treatment vs. vehicle-WT/pre-treatment, p=0.0477; THC-D_1R-Cre/pre-treatment vs. THC-WT/pre-treatment, p=0.0450) (***Figure 6B***).

Taken together, all these findings indicate that CB_1 receptors located on D_1R-MSNs, but not on corticostriatal projections, are required for the autophagy-inhibiting and motor-dyscoordinating activity of THC.

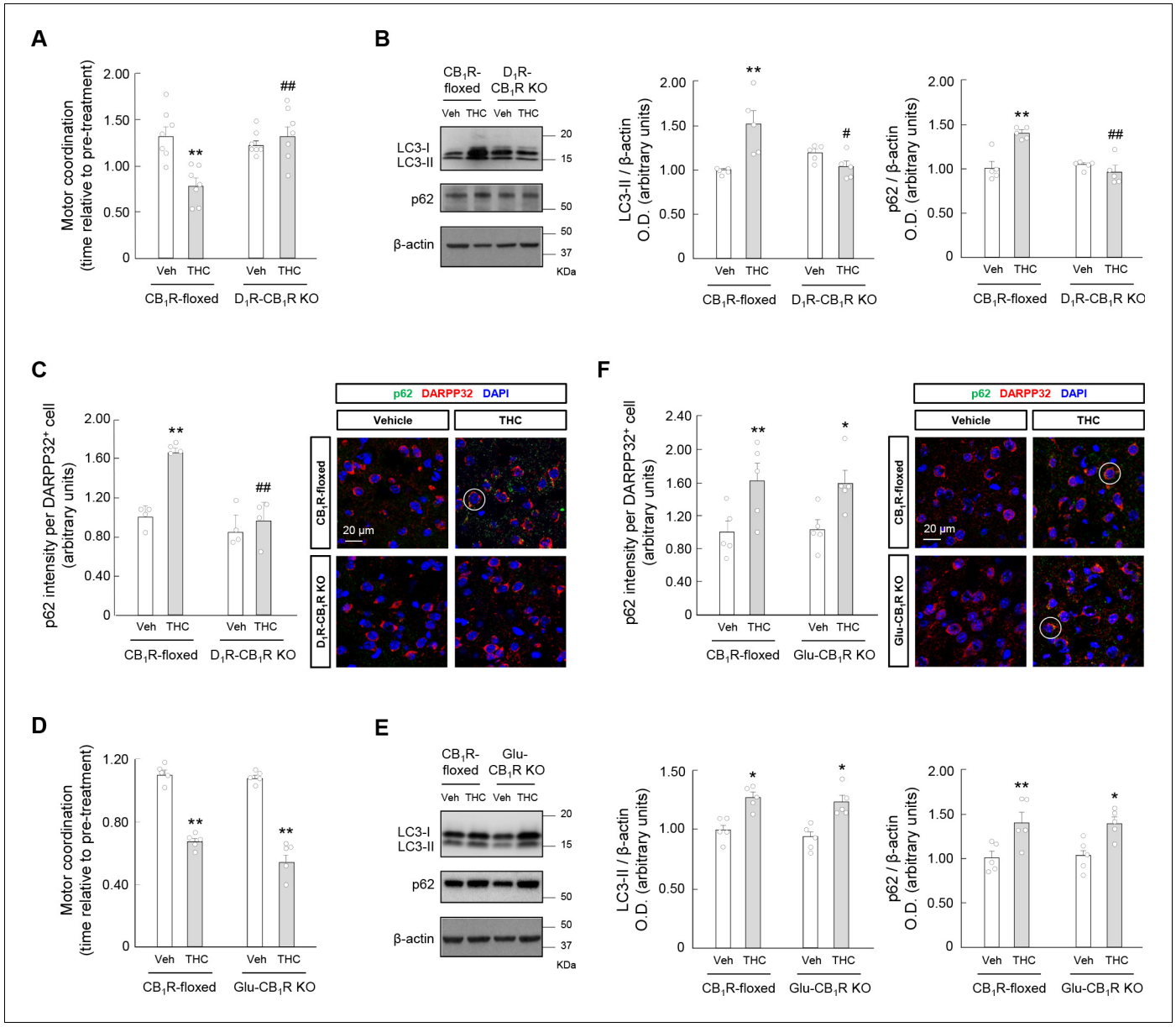

Figure 5. Cannabinoid CB_1 receptors located on D_1R-MSNs, but not on glutamatergic neurons, are required for the THC-induced impairment of striatal autophagy and motor coordination in vivo. (**A–C**) D_1R-CB_1R KO mice and CB_1R-floxed control littermates were treated with THC (10 mg/kg as a single i.p.injection) or its vehicle for 4 hr. *Panel A*, Motor coordination (RotaRod test, time to fall relative to pre-treatment; *n* = 7 animals per group). *Panel B*, Western blot analysis of autophagy markers in the striatum. Representative blots of each condition, together with optical density values relative to those of loading controls, are shown (*n* = 5 animals per group). Blots were cropped for clarity. Electrophoretic migration of molecular weight markers is depicted on the right-hand side of each blot. *Panel C*, Immunofluorescence analysis of p62 (p62 fluorescence intensity per DARPP32-positive cell) in the dorsal striatum (*n* = 4 animals per group). Representative images with an encircled example of high-intensity cell are shown. (**D–F**) Glu-CB_1R KO mice and CB_1R-floxed control littermates were treated with THC (10 mg/kg as a single i.p. injection) or its vehicle for 4 hr. *Panel D*, Motor coordination (RotaRod test, time to fall relative to pre-treatment; *n* = 5 animals per group). *Panel E*, Western blot analysis of autophagy markers in the striatum. Representative blots of each condition, together with optical density values relative to those of loading controls, are shown (*n* = 5 animals per group). Blots were cropped for clarity. Electrophoretic migration of molecular weight markers is depicted on the right-hand side of each blot. *Panel F*, Immunofluorescence analysis of p62 (p62 fluorescence intensity per DARPP32-positive cell) in the dorsal striatum (*n* = 4 animals per group). Representative images with an encircled example of high-intensity cell are shown. *p<0.05, **p<0.01 from the corresponding vehicle-treated group, or $^{\#}$p<0.05, $^{\#\#}$p<0.01 from the corresponding THC-treated CB_1R-floxed group, by two-way ANOVA with Tukey's multiple comparisons test. Raw numerical data and further statistical details are shown in ***Figure 5—source data 1***.

The online version of this article includes the following source data and figure supplement(s) for figure 5:

Figure 5 continued on next page

Figure 5 continued

Source data 1. Source data for Cannabinoid CB_1 receptors located on D_1R-MSNs, but not on glutamatergic neurons, are required for the THC-induced impairment of striatal autophagy and motor coordination in vivo.
Figure supplement 1. Rimonabant rescues THC-induced motor dyscoordination.

Discussion

Here, we identify impairment of autophagy as an unprecedented mechanism involved in cannabinoid-induced motor alterations. On molecular grounds, our data favour a 'two-hit' model by which engagement of striatal CB_1 receptors may impair autophagy. First, CB_1 receptor activation, by coupling to the phosphatidylinositol-3-kinase/Akt/mTORC1 pathway, would lead to ULK1 phosphorylation, which, subsequently, would inhibit autophagosome formation/autophagy initiation. Second, CB_1 receptor activation, by a hitherto undefined mechanism that may conceivably involve an impact on lysosomal function (***Hiebel and Behl, 2015***), would inhibit autophagosome clearance/autophagy completion. We are aware, however, that our work has several shortcomings that could limit the generalization of its conclusions. Specifically, (*i*) the data (except for the cell-culture experiments) come from a single cannabinoid agonist (THC) given at a single dose (10 mg/kg, i.p.), and were collected at a single time point after administration (4 hr); (*ii*) only two (albeit well-established) motor behavior measures were examined (RotaRod and open field); and (*iii*) only male animals were studied.

By targeting mTORC1 with temsirolimus, we report a feasible pharmacological intervention to rescue the concerted THC-evoked impairment of autophagy and motor coordination. Temsirolimus prevents other unwanted effects of THC, such as short-term memory loss and anxiety, leaving potential therapeutically sought cannabinoid actions as analgesia and anxiolysis unaffected (***Puighermanal et al., 2013***). Temsirolimus has similar potency and specificity for mTOR than rapamycin, but longer stability and increased solubility, and is already approved by the FDA as first-line treatment for metastatic renal cancer patients classified as poor risk (***Hudes et al., 2007***). In these patients, temsirolimus is well-tolerated, increases overall survival, and improves quality of life (***Zanardi et al., 2015***). Taken together, these pieces of evidence suggest that administration of temsirolimus, or other FDA-approved rapalogs like everolimus (***Janku et al., 2018***; ***Lebwohl et al., 2013***), might help to counteract some particular unwanted effects of cannabis.

Dietary manipulation with trehalose also prevented the THC-evoked impairment of autophagy and motor dyscoordination. Trehalose, a nontoxic disaccharide found in numerous plants, microorganisms and invertebrates, contains an $\alpha,\alpha-1,1$-glucoside bond between two α-glucose units, thus being an extremely stable sugar. In many countries, including USA, trehalose is added to various food products as nutritional supplement and 'natural flavor' (***Richards et al., 2002***). On physiological grounds, trehalose is believed to stabilize proteins and to protect them from stress-induced unfolding, aggregation and degradation (***Emanuele, 2014***; ***Hosseinpour-Moghaddam et al., 2018***). Vertebrates cannot synthesize trehalose, but exogenous trehalose administration induces the clearance of toxic protein aggregates in cultured mammalian cells, and exerts therapeutic effects in a plethora of mouse models of protein-misfolding disorders (including Huntington's disease, Alzheimer's disease, Parkinson's disease and amyotrophic lateral sclerosis) concomitantly to autophagy induction (***Hosseinpour-Moghaddam et al., 2018***; ***Menzies et al., 2017***). Although its mechanism of action is not completely understood (***Lee et al., 2018***), trehalose has been proposed to activate autophagy via competitive inhibition of GLUT glucose transporters, thus impairing cellular energy supply and stimulating AMPK (***DeBosch et al., 2016***). In our hands, however, the phosphorylation state of the main AMPK-dependent site in ULK1 remained unaffected upon trehalose treatment. We also observed that, in line with some reports (e.g. ***Sarkar et al., 2007***), trehalose did not affect the basal activity of mTORC1-pathway molecular markers; and, in line with other reports (e.g. ***DeBosch et al., 2016***), it attenuated stimulus-evoked mTORC1 overactivation. Thus, it is likely that AMPK, mTORC1, and the contextual crosstalk between these two pivotal signalling axes (***Alers et al., 2012***) are required for the full pro-autophagic effects of trehalose to be observed.

We also define here the neuroanatomical basis for the autophagy-inhibiting and motor-dyscoordinating actions of THC. The CB_1 receptor is one of the most abundant metabotropic receptors in the striatum, where it is mainly expressed in D_1R-MSNs, D_2R-MSNs, GABAergic interneurons, and

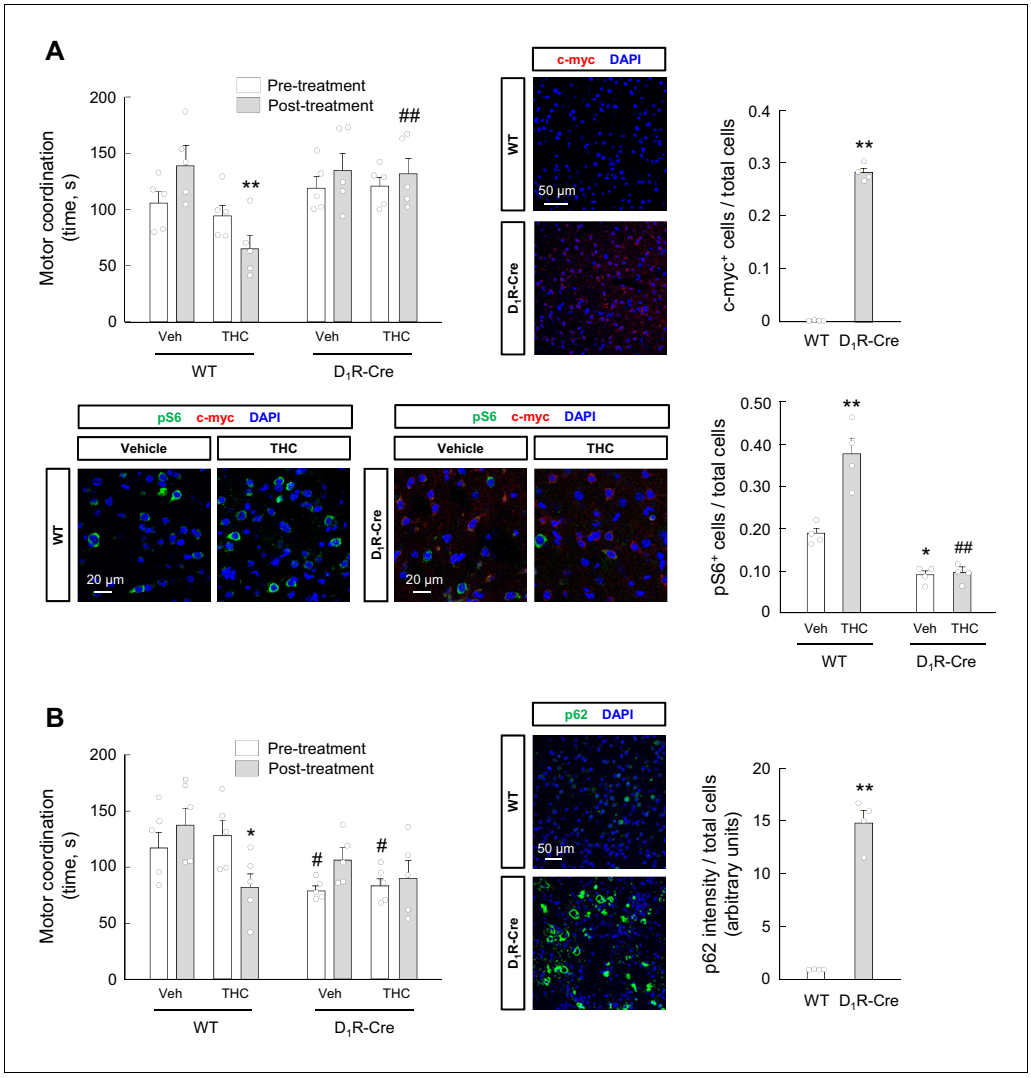

Figure 6. mTORC1 and p62 in D_1R-MSNs participate in the THC-induced impairment of motor coordination in vivo. (**A**) D_1R-Cre mice and wild-type control littermates were injected stereotactically into the dorsal striatum with a CAG-DIO-dnRaptor rAAV, and left untreated for 4 weeks. Animals were subsequently treated with THC (10 mg/kg as a single i.p. injection) or its vehicle for 4 hr, and motor coordination was evaluated (RotaRod test, time to fall in seconds; *n* = 5 animals per group). **p<0.01 from vehicle-treated WT/post-treatment group, or $^{\#\#}$p<0.01 from THC-treated WT/post-treatment group, by two-way ANOVA with Tukey's multiple comparisons test. Representative images of c-myc tag and phosphorylated ribosomal protein S6 staining in the dorsal striatum, together with their quantification (c-myc-positive cells relative to total cells, or phospho-S6-positive cells relative to total cells), are shown (*n* = 4 animals per group). **p<0.01 from WT group by unpaired Student *t*-test (*c-myc immunofluorescence*); *p<0.05, **p<0.01 from vehicle-treated/WT group, or $^{\#\#}$p<0.01 from THC-treated/WT group, by two-way ANOVA with Tukey's multiple comparisons test (*phospho-S6 immunofluorescence*). (**B**) D_1R-Cre mice and wild-type control littermates were injected stereotactically into the dorsal striatum with a CAG-DIO-p62 rAAV, and left untreated for 4 weeks. Animals were subsequently treated with THC (10 mg/kg as a single i.p. injection) or its vehicle for 4 hr, and motor coordination was evaluated (RotaRod test, time to fall in seconds; *n* = 5 animals per group). *p<0.05 from vehicle-treated WT/post-treatment group, or $^{\#}$p<0.05 from the respective WT/pre-treatment group, by two-way ANOVA with Tukey's multiple comparisons test. Representative images of p62 staining in the dorsal striatum, together with their quantification (p62 fluorescence intensity relative to total cells), are shown (*n* = 4 animals per group). **p<0.01 from WT group by unpaired Student *t*-test. Raw numerical data and further statistical details are shown in ***Figure 6—source data 1***.

The online version of this article includes the following source data and figure supplement(s) for figure 6:

Source data 1. Source data for mTORC1 and p62 in D_1R-MSNs participate in the THC-induced impairment of motor coordination in vivo.

Figure 6 continued on next page

Figure 6 continued

Figure supplement 1. THC activates the mTORC1 pathway in D_1R-MSNs but not D_2R-MSNs in vivo.

astrocytes, as well as in glutamatergic terminals projecting from the cortex (***Castillo et al., 2012***; ***Davis et al., 2018***; ***Uchigashima et al., 2007***). This complex anatomical profile dictates an intricate repertoire of modulatory actions controlled by endocannabinoids through different CB_1 receptor pools, ranging from synaptic plasticity (***Covey et al., 2017***; ***Kreitzer, 2009***) to astrocyte-neuron communication (***Araque et al., 2017***) and neuronal integrity (***Chiarlone et al., 2014***; ***Naydenov et al., 2014***). Specifically, our data show that the pool of CB_1 receptors located on D_1R-MSNs plays an indispensable role in cannabinoid-induced impairment of autophagy and motor coordination. Of note, it has been shown that this precise CB_1 receptor subpopulation is also necessary for cannabinoid-induced catalepsy, although not for overall cannabinoid-induced hypomotility (***Monory et al., 2007***), thus supporting that, in agreement with our data, it controls selected aspects of motor behavior. In addition, CB_1 receptors located on corticostriatal terminals, by controlling glutamatergic signalling, contribute to THC-induced hypolocomotion (***Monory et al., 2007***), participate in endocannabinoid-dependent long-term depression as evoked by D_1R-MSNs (***Bagetta et al., 2011***; ***Wu et al., 2015***) and protect D_1R-MSNs from toxic insults (***Ruiz-Calvo et al., 2018***). Thus, endocannabinoid signalling fine-tunes the functions and viability of D_1R-MSNs through a delicate armamentarium of CB_1 receptor pools located on both D_1R-MSNs, presynaptic terminals impinging on them, and other surrounding cell types.

We note that our work does not unveil the precise cellular and molecular mechanisms by which the CB_1 receptor-evoked inhibition of autophagy in D_1R-MSNs affects brain functionality to change motor coordination. Neuronal communication is finely sensitive to proteostatic processes as autophagy, which, for example, clears dysfunctional proteins and fine-tunes the trafficking/recycling of membrane neurotransmitter receptors (e.g. ionotropic glutamate receptors; ***Birdsall and Waites, 2019***). Neuronal activity is associated to the mTORC1 pathway and autophagy, and this could in turn participate in NMDA receptor-dependent synaptic plasticity and brain function (***Shehata et al., 2012***). Hence, the control of long-term depression exerted by CB_1 receptors on D_1R-MSNs (***Bagetta et al., 2011***; ***Wu et al., 2015***) might be mechanistically connected to the THC-evoked effects on mTORC1/autophagy reported here, perhaps by signaling in a cell-autonomous manner through the accumulation of the multifunctional scaffold protein p62 (***Sánchez-Martín and Komatsu, 2018***). These possibilities notwithstanding, our findings might also be relevant in other neurobiological processes that are known to be controlled by the striatum and impacted by cannabinoids - for example cognition, affection and reward (***Katona and Freund, 2008***; ***Kreitzer, 2009***; ***Lovinger, 2010***). Moreover, from a translational point of view, it is tempting to speculate that D_1R-MSNs, but not corticostriatal terminals, would constitute the neuroanatomical target of strategies aimed at managing some specific cannabis-induced behavioral alterations as catalepsy and dyscoordination.

Materials and methods

Key resources table

Reagent type (species) or resource	Designation	Source or reference	Identifiers	Additional information
Strain, strain background (*Mus musculus*, C57BL/6N, male)	*Cnr1*$^{fl/fl}$;*Drd1a*^{Cre}	***Monory et al., 2007***; doi:10.1371/journal.pbio.0050269	N/A	Conditional mutant mice in which the CB_1 receptor gene (*Cnr1*) is absent from D_1R (*Drd1a*)-expressing cells
Strain, strain background (*Mus musculus*, C57BL/6N, male)	*Drd1a*^{Cre}	***Lemberger et al., 2007***; doi:10.1186/1471-2202-8-4	N/A	Transgenic mice expressing Cre recombinase in D_1R (*Drd1a*)-expressing cells

Continued on next page

Continued

Reagent type (species) or resource	Designation	Source or reference	Identifiers	Additional information
Strain, strain background (*Mus musculus*, C57BL/6N, male)	*Cnr1*$^{fl/fl}$;*Neurod6*^{Cre}	**Monory et al., 2006**; doi:10.1016/j.neuron.2006.07.006	N/A	Conditional mutant mice in which the CB_1 receptor gene (*Cnr1*) is absent from dorsal telencephalic glutamatergic (*Neurod6*-expressing) neurons
Strain, strain background (*Mus musculus*, C57BL/6N, male)	*Drd1a-tdTomato; Drd2-EGFP*	**Suárez et al., 2014**; doi:10.1016/j.biopsych.2013.05.006	N/A	Transgenic mice expressing the tdTomato and EGFP reporter genes under the control of the *Drd1a* gene promoter and the *Drd2* gene promoter, respectively
Strain, strain background (*Mus musculus*, C57BL/6N, male)	C57BL/6N	Harlan Laboratories	RRID:MGI:5902763	Wild-type mice
Transfected construct (*Homo sapiens*)	Myc-Raptor (ΔCT) expression vector	Addgene **Hara et al., 2002**; doi:10.1016/s0092-8674(02)00833–4. **Koketsu et al., 2008**; doi:10.1152/ajpendo.00253.2007	Plasmid #1859; RRID:Addgene_1859	Vector backbone: pRK-5; construct generated by PCR-mediated deletion of 1293 base pairs at the Raptor C-terminus
Transfected construct (*Homo sapiens*)	HA-p62 expression vector	Addgene	Plasmid #28027; RRID:Addgene_28027	Vector backbone: pcDNA4/TO
Genetic reagent (*Homo sapiens*)	CAG-DIO rAAV expression vector	**Klugmann et al., 2005**; doi:10.1016/j.mcn.2004.10.002 **Bellocchio et al., 2016**; doi:10.1523/JNEUROSCI.1192–16.2016	CAG-DIO rAAV Hybrid serotype 1/2	Recombinant adeno-associated virus (rAAV) for Cre-driven transgene expression with a CAG promoter
Biological sample (*Mus musculus*)	Primary striatal neurons	Harlan Laboratories (C57BL/6N mice)	C57BL/6N RRID:MGI:5902763	In vitro cell cultures
Antibody	Anti-LC3B (rabbit polyclonal)	Sigma-Aldrich	Cat. #L7543; RRID:AB_796155	IF (1:300); WB (1:4000)
Antibody	Anti-p62 (rabbit polyclonal)	Enzo Life Sciences	Cat. #BML-PW9860-0025; RRID:AB_2052149	IF (1:250); WB (1:1000)
Antibody	Anti-p62 (rabbit polyclonal)	Progen	Cat. #GP62-C; RRID:AB_2687531	WB (1:1000)
Antibody	Anti-LAMP1 (rabbit polyclonal)	Abcam	Cat. #ab25245 RRID:AB_449893	IF (1:1000)
Antibody	Anti-DARPP32 (mouse monoclonal)	BD Biosciences	Cat. #611520; RRID:AB_398980	IF (1:700)
Antibody	Anti-phospho-S6-S235/S236 (rabbit polyclonal)	Cell Signaling	Cat. #2211; RRID:AB_331679	IF (1:300)
Antibody	Anti-phospho-S6-S240/S244 (rabbit polyclonal)	Cell Signaling	Cat. #5364; RRID:AB_10694233	IF (1:800)
Antibody	Anti-c-Myc (mouse monoclonal)	Sigma-Aldrich	Cat. #11-667-149-001; RRID:AB_390912	IF (1:500)
Antibody	Anti-phospho-S6K-T389 (mouse monoclonal)	Cell Signaling	Cat. #9206; RRID:AB_2285392	WB (1:1000)
Antibody	Anti-total-S6K (rabbit polyclonal)	Cell Signaling	Cat. #9202; RRID:AB_331676	WB (1:1000)

Continued on next page

Continued

Reagent type (species) or resource	Designation	Source or reference	Identifiers	Additional information
Antibody	Anti-phospho-ULK1-S757 (rabbit polyclonal)	Cell Signaling	Cat. #6888; RRID:AB_10829226	WB (1:1000)
Antibody	Anti-phospho-ULK1-S555 (rabbit polyclonal)	Cell Signaling	Cat. #5869; RRID:AB_10707365	WB (1:1000)
Antibody	Anti-total-ULK1 (rabbit polyclonal)	Cell Signaling	Cat. #8054; RRID:AB_11178668	WB (1:1000)
Antibody	Anti-β-actin (mouse monoclonal)	Sigma-Aldrich	Cat. #A5441; RRID:AB_476744	WB (1:4000)
Antibody	Anti-mouse monoclonal IgG (HRP-linked whole antibody)	GE-Healthcare Lifescience	Cat. #NA931; RRID:AB_772210	WB (1:5000)
Antibody	Anti-rabbit monoclonal IgG (HRP-linked whole antibody)	GE-Healthcare Lifescience	Cat. #NA934; RRID:AB_2722659	WB (1:5000)
Antibody	Goat anti-guinea pig IgG (H+L) (HRP-linked secondary antibody)	Invitrogen	Cat. #A18769; RRID:AB_2535546	WB (1:5000)
Antibody	Goat anti-mouse IgG (H+L) (cross-adsorbed, Alexa Fluor 488)	Invitrogen	Cat. #A-11001; RRID:AB_2534069	IF (1:500)
Antibody	Goat anti-mouse IgG (H+L) (cross-adsorbed, Alexa Fluor 594)	Invitrogen	Cat. #A-11005; RRID:AB_2534073	IF (1:500)
Antibody	Goat anti-mouse IgG (H+L) (cross-adsorbed, Alexa Fluor 647)	Invitrogen	Cat. #A-21235; RRID:AB_2535804	IF (1:500)
Antibody	Goat anti-rabbit IgG (H+L) (cross adsorbed, Alexa Fluor 488)	Invitrogen	Cat. #A-11008; RRID:AB_143165	IF (1:500)
Antibody	Goat anti-rabbit IgG (H+L) (cross adsorbed, Alexa Fluor 594)	Invitrogen	Cat. #A-11012; RRID:AB_2534079	IF (1:500)
Antibody	Goat anti-rabbit IgG (H+L) (cross adsorbed, Alexa Fluor 647)	Invitrogen	Cat. #A-21244; RRID:AB_2535812	IF (1:500)
Commercial assay or kit	Papain dissociation system (PDS)	Worthington	Cat. #LK 003153	In vitro cell cultures
Chemical compound, drug	Δ^9-tetrahydro-cannabinol (THC)	THC Pharm GmbH	Dronabinol	In vivo experiments (10 mg/kg, i.p.); in vitro experiments (0.75 µM)
Chemical compound, drug	Rimonabant (SR141716)	Cayman Chemical	Cat. #9000484	In vivo experiments: (3 mg/kg, i.p.)
Chemical compound, drug	Temsirolimus	LC Labs	Cat. #T-8040	In vivo experiments (1 mg/kg, i.p.)

Continued on next page

Continued

Reagent type (species) or resource	Designation	Source or reference	Identifiers	Additional information
Chemical compound, drug	Trehalose	Merck-Calbiochem	Cat. #90210	In vivo experiments (10 g/L in drinking water)
Chemical compound, drug	HU-210	Tocris	Cat. #0966	In vitro experiments (10 nM)
Chemical compound, drug	Hydroxychloroquine	Merck	Cat. #509272	In vitro experiments (0.1 mM)
Chemical compound, drug	E64d	Enzo Life Sciences	Cat. #BML-PI107-0001	In vitro experiments (0.1 µM)
Chemical compound, drug	Pepstatin A	Enzo Life Sciences	Cat. #ALX -260–085 M005	In vitro experiments (10 ng/ml)
Software, algorithm	Graph Pad Prism 8.0	GraphPad Software Inc	RRID:SCR_002798	Descriptive analysis and statistics
Software, algorithm	IBM SPSS	IBM Corporation	RRID:SCR_002865	Statistical power analysis
Software, algorithm	Image J	NIH	RRID:SCR_003070	Western blot and immune-microscopy image analysis
Software, algorithm	TCS-SP8 Leica Application Suite X, LASX	Leica	RRID:SCR_013673	SP8 AOBS confocal microscopy image capture
Software, algorithm	ACTITRACKUPG V2.7	Panlab	Cat. #76–0610	Motor activity analysis
Other	DAPI stain	Invitrogen	Cat. #D1306; RRID:AB_2629482	IF (1 µg/mL)
Other	RotaRod LE8200	Harvard Apparatus	Cat. #LE8200 (76–0237)	Motor coordination testing
Other	IR actimeter (ActiTrack)	Panlab	Cat. #76–0127, #76–0131, #76–0134, #76–0125	Motor activity testing

Animals

We used conditional mutant mice, generated by the Cre-loxP technology, in which the CB_1 receptor gene (*Cnr1*) is absent either from D_1R-expressing neurons (*Cnr1*$^{fl/fl}$ mice bred with *Drd1a*^{Cre} mice; referred to here as D_1R-CB_1R KO mice) (**Monory et al., 2007**) or from dorsal telencephalic glutamatergic neurons (*Cnr1*$^{fl/fl}$ mice bred with *Neurod6*^{Cre} mice; referred to here as Glu-CB_1R KO mice) (**Monory et al., 2006**), as well as their respective *Cnr1*$^{fl/fl}$ (referred to here as CB_1R-floxed) littermates. We also used BAC transgenic mice expressing the tdTomato and EGFP reporter genes under the control of the *Drd1a* gene promoter and *Drd2* gene promoter, respectively (*Drd1a-tdTomato; Drd2-EGFP* mice; colony founders kindly provided by Rosario Moratalla, Cajal Institute, Madrid, Spain) (**Suárez et al., 2014**). Wild-type C57BL/6N mice were purchased from Harlan Laboratories (Barcelona, Spain). Animal housing, handling and assignment to the different experimental groups were conducted essentially as described before (**Bagetta et al., 2011**). Throughout the study, animals had unrestricted access to food and water. They were housed (4–5 mice per cage) under controlled temperature (range, 20–22˚C), humidity (range, 50–55%) and light/dark cycle (light between 8:00 am and 8:00 pm). Animals were habituated to housing conditions before the start of the experiments, were assigned randomly to the different treatment groups, and all experiments were performed in a blinded manner for genotype, pharmacological treatment and viral injection. All animals used in the experiments were male adults (*ca.* 8-week-old). Adequate measures were taken to minimize pain and discomfort of the animals, as well as the number of animals used in the experiments, on the basis of the 3Rs (replacement, reduction and refinement) principle. Mice were sacrificed either by intracardial perfusion with paraformaldehyde (and their brains subsequently excised for histological analyses) or by cervical dislocation (and their striata, or other brain regions, subsequently dissected for Western blot analyses). All the experimental procedures were performed in accordance with the guidelines and with the approval of the Animal Welfare Committee of Universidad

Complutense de Madrid and Comunidad de Madrid (PROEX 209/18), and in accordance with the directives of the European Commission (2010/63/EU).

Drug treatments in vivo

THC (THC Pharm GmbH, Frankfurt am Main, Germany) and SR141716 (rimonabant; Cayman Chemical, Ann Arbor, MI, USA) were stored in DMSO. Just before the experiments, solutions of vehicle [1% (v/v) DMSO in Tween-80/saline (1:80, v/v)], THC (10 mg/kg body weight) and/or rimonabant (3 mg/kg body weight) were prepared for i.p. injections. When rimonabant was used (***Figure 5—figure supplement 1***), mice were treated with rimonabant (3 mg/kg as a single i.p. injection) or vehicle for 20 min, and, subsequently, with THC (10 mg/kg as a single i.p. injection) or vehicle for 4 hr. Temsirolimus (LC Labs, Woburn, MA, USA) was prepared fresh in DMSO just before the experiments. Mice were treated with temsirolimus (1 mg/kg as a single i.p. injection) or its vehicle for 20 min, and, subsequently, with THC (10 mg/kg as a single i.p. injection) or its vehicle for 4 hr. Trehalose (Merck-Calbiochem, Barcelona, Spain) was directly added to the drinking water of the animals. Mice were given trehalose (10 g/L) or plain water ad libitum for 24 hr, and, subsequently, were treated with THC (10 mg/kg as a single i.p. injection) or its vehicle for 4 hr. Under these conditions, the addition of trehalose did not affect the volume of water that was drunk by the animals. The doses of temsirolimus and trehalose used were selected from both previous studies (***Puighermanal et al., 2013***; ***Rodríguez-Navarro et al., 2010***) and pilot experiments on motor behavior.

Viral vectors

The coding sequence of dominant-negative Raptor with a c-Myc tag (Myc-RaptorΔCT) was generated by PCR-mediated deletion of 1293 base pairs at the *C*-terminus (***Hara et al., 2002***) of wild-type Myc-tagged Raptor (Addgene, Watertown, MA; plasmid #1859) (***Koketsu et al., 2008***). Myc-RaptorΔCT or human HA-tagged p62 (Addgene; plasmid #28027) was subcloned in a CAG-DIO rAAV vector, to allow the Cre-dependent expression of the transgene, by using standard molecular biology techniques. The vectors used were of an AAV1/AAV2-mixed serotype and were generated by calcium phosphate transfection of HEK-293T cells (American Type Culture Collection, Manassas, VA) and subsequent purification, as described previously (***Bellocchio et al., 2016***). Wild-type and D_1R-Cre mice were injected stereotactically with the rAAV vector into the dorsal striatum. Each animal received one bilateral injection at the following coordinates (to bregma): antero-posterior +0.5, lateral ±2.0, dorso-ventral −3.0 (***Bellocchio et al., 2016***). Mice were left untreated for 4 weeks to attain transgene expression before being subjected to the behavioral tests.

Neuronal cultures

Primary striatal neurons were obtained from 0 to 1-day-old C57BL/6N mice using a papain dissociation system (Worthington, Lakewood, NJ) (***Blázquez et al., 2015***). Striata were dissected, and cells were seeded at 200,000 cells/cm^2 on plates that had been pre-coated with 0.1 mg/mL poly-D-lysine, in Neurobasal medium supplemented with B27 and Glutamax. Cultures were maintained for 7 days in vitro to allow neuronal differentiation. They were subsequently incubated for 24 hr with THC (0.75 µM; THC Pharm GmbH) or HU-210 (10 nM; Tocris; Bristol, UK), alone or in combination with hydroxychloroquine (0.1 mM; Merck, Barcelona, Spain) or E64d (0.1 µM; Enzo Life Sciences, Barcelona, Spain) plus pepstatin A (10 ng/ml; Enzo Life Sciences), or vehicle [DMSO, 0.1–0.2% (v/v) final concentration], before they were fixed for immunomicroscopy. Within each neuronal preparation, incubations were conducted in triplicate for every vehicle or drug condition. The total number of experimental conditions assayed within each neuronal preparation depended on the cell yield of that particular preparation.

Immunomicroscopy

Cells were cultured on coverslips and fixed in 4% paraformaldehyde. Coronal free-floating sections (30 µm-thick) were obtained from paraformaldehyde-perfused mouse brains. Samples were first incubated with 10% goat serum in PBS supplemented with 0.25% Triton X-100 for 1 hr at room temperature to block non-specific binding, and subsequently stained overnight at 4˚C with antibodies against LC3 (1:300; Sigma-Aldrich, St. Louis, MO, #L7543), p62 (1:250; Enzo Life Sciences, #BML-PW9860-0025), LAMP1 (1:1000; Abcam, Cambridge, UK, #ab25245), DARPP32 (1:700; BD

Biosciences, Franklin Lakes, NJ, #611520), phosphorylated ribosomal protein S6-S235/S236 [1:300; Cell Signaling, Danvers, MA, #2211; similar data were obtained in pilot experiments when an antibody directed against two other mTORC1/S6K-phosphorylated residues of ribosomal protein S6 (S240/S244) was used (1:800; Cell Signaling, #5364)] or c-Myc (1:500; Sigma-Aldrich, #11-667-149-001), followed by the corresponding Alexa Fluor-conjugated secondary antibodies (1:500; 1.5 hr, room temperature, darkness; Invitrogen, Madrid, Spain, #A-11001, #A-11005, #A-21235; #A-11008, #A-11012, #A-21244). Three washes (20 min each) with 1% goat serum in PBS supplemented with 0.25%Triton X-100 were conducted both between antibody incubations and before sample mounting. Nuclei were visualized with DAPI. Analysis of marker-protein immunoreactivity in the dorsal striatum was conducted in a 1-in-10 series per animal (from bregma +1.5 to −0.5 coronal coordinates). A total of 6–8 sections (comprising 2–3 fields per section) was analyzed per mouse brain. For LC3, data were calculated as number of cells with three or more LC3-positive dots. For p62, data were calculated as immunofluorescence intensity. For DARPP32, LAMP1, c-Myc and phosphorylated ribosomal protein S6, data were calculated as number of positive cells. For tdTomato and EGFP fluorescence in *Drd1a-tdTomato/Drd2-EGFP* mice, data were calculated as number of positive cells. Confocal fluorescence images were acquired using TCS-SP8 (Leica Application suite X, LASX) software and a SP8 AOBS microscope (Leica, Wetzlar, Germany). Inclusive fluorescence thresholds were set at an average of 105 (low) and 255 (high). Images were analyzed with ImageJ software (NIH, Bethesda, MA). All immunomicroscopy analyses relied on an unbiased quantification of ImageJ-positive pixels, and were conducted in a blinded manner for genotype, pharmacological treatment and viral injection.

Western blot

Western blot experiments were conducted with antibodies raised against LC3 (1:4000; Sigma-Aldrich, #L7543), p62 [1:1000; Enzo Life Sciences, #BML-PW9860-0025; similar data were obtained in pilot experiments when a different anti-p62 antibody was used (1:1000; Progen, Heidelberg, Germany, #GP62-C)], phosphorylated S6K-T389 (1:1000; Cell Signaling, #9206), total S6K (1:1000; Cell Signaling, #9202), phosphorylated ULK1-S757 (1:1000; Cell Signaling, #6888), phosphorylated ULK1-S555 (1:1000; Cell Signaling, #5869), total ULK1 (1:1000; Cell Signaling, #8054) or β-actin (1:4000, Sigma-Aldrich, #A5441), followed by the corresponding HRP-linked secondary antibodies (1:5000; GE-Healthcare, Madrid, Spain, #NA931; GE-Healthcare, #NA934; Invitrogen, #A18769), as appropriate. Densitometric analysis was performed with Image J software (NIH).

Motor behavior

Motor coordination analysis (RotaRod test) was conducted with acceleration from 4 to 40 r.p.m. over a period of 600 s in an LE8200 device (Harvard Apparatus, Barcelona, Spain) (***Blázquez et al., 2011***). Any mouse remaining on the apparatus after 600 s was removed, and its time was scored as 600 s. RotaRod performance was evaluated in two phases. First, before any pharmacological treatment, naive mice were tested on three consecutive days, for three trials per day, with a rest period of 40 min between trials. Data from the three trials conducted on the first day were not used in statistical analyses, as they merely reflect the initial contact of the animal with the RotaRod device (***Hockly et al., 2003***). Data from the three trials conducted on the second day plus the three trials conducted on the third day were averaged for each animal, so constituting the herein referred to as 'pre-treatment' RotaRod performance. Second, on the day of the pharmacological experiment, 4 hr after vehicle or drug treatment, mice were tested for three trials, with a rest period of 40 min between trials. Data from these three trials were averaged for each animal, so constituting the herein referred to as 'post-treatment' RotaRod performance. Hence, for each animal, its 'post-treatment' RotaRod performance was compared with its 'pre-treatment' RotaRod performance. Motor activity analysis was conducted in an automated actimeter consisting of a 22.5 × 22.5 cm area with 16 surrounding infrared beams coupled to a computerized control unit (ActiTrack; Panlab, Barcelona, Spain) (***Blázquez et al., 2011***). Four hours after vehicle or drug treatment, animals were recorded once for a period of 10 min, in which total distance travelled (cm), overall activity (counts), resting time (s), fast movements (counts) and stereotypic movements (counts) were measured.

Statistics

Unless otherwise specified, data are presented as mean ± SEM of the number of animals or independent neuronal preparations indicated in each case. Statistical comparisons were made by unpaired Student *t*-test, or by ANOVA followed by Tukey's multiple comparisons test, as indicated in each figure legend. For clarity, only p values lower than 0.05 were considered statistically significant. The source data files include all raw numerical data as well as further details of the statistical analyses, which were carried out with GraphPad Prism 8.0 software (San Diego, CA). Power analysis was conducted with IBM SPSS software (IBM France, Bois-Colombes, France).

Acknowledgements

This work was supported by the Spanish *Ministerio de Ciencia, Innovación y Universidades* (MCIU/FEDER; grants SAF2015-64945-R and RTI2018-095311-B-I00 to MG, and SAF2016-78666-R to JARN). AR-C was supported by a contract from the Spanish *Ministerio de Ciencia, Innovación y Universidades* (MCIU/FEDER; *Formación de Personal Investigador* Program). RB-G was supported by a contract from the Spanish *Ministerio de Ciencia, Innovación y Universidades* (MCIU/FEDER; *Juan de la Cierva* Program). GM and LB were supported by INSERM. GM was also supported by *Fondation pour la Recherche Medicale* (grants DRM20101220445 and DPP20151033974), Human Frontiers Science Program (grant RGP0036/2014), European Research Council (Endofood grant ERC-2010-StG-260515, CannaPreg grant ERC-2014-PoC-640923, and MiCaBra grant ERC-2018-AdG-786467), *Region Nouvelle Aquitaine*, and *Agence Nationale de la Recherche* (ANR Blanc MitObesity grant ANR-18-CE14-0029-01, ANR LabEx BRAIN grant ANR-10-LABX-0043, ANR Blanc ORUPS grant ANR-16-CE37-0010-01, and ANR Blanc CaCoVi grant ANR 18-CE16-0001-02). LB was also supported by *Fondation pour la Recherche Medicale* (grant ARF20140129235) and *Agence Nationale de la Recherche* (ANR Blanc mitoCB1-fat grant ANR-19-CE14). We are indebted to E García-Taboada, L Rivera, A Gaudioso, P García-Rozas, and MJ Asensio for expert laboratory assistance; D Gonzales, N Aubailly, and all the personnel from the animal facilities of the NeuroCentre Magendie; M Biguerie from the technical service of the NeuroCentre Magendie; all the personnel from the Bordeaux Imaging Center; and V Morales for continuous help.

Additional information

Funding

Funder	Grant reference number	Author
Spanish Ministerio de Ciencia, Innovación y Universidades	SAF2015-64945-R	Manuel Guzmán
Spanish Ministerio de Ciencia, Innovación y Universidades	RTI2018-095311-B-I00	Manuel Guzmán
Spanish Ministerio de Ciencia, Innovación y Universidades	SAF2016-78666-R	José A Rodríguez-Navarro
Fondation pour la Recherche Médicale	DRM20101220445	Giovanni Marsicano
Fondation pour la Recherche Medicale	DPP20151033974	Giovanni Marsicano
Human Frontier Science Program	RGP0036/2014	Giovanni Marsicano
H2020 European Research Council	ERC-2010-StG-260515	Giovanni Marsicano
H2020 European Research Council	ERC-2014-PoC-640923	Giovanni Marsicano
H2020 European Research Council	ERC-2018-AdG-786467	Giovanni Marsicano
Region Nouvelle Aquitaine		Giovanni Marsicano

Agence Nationale de la Recherche	ANR-16-CE37-0010-01	Giovanni Marsicano
Agence Nationale de la Recherche	ANR 18-CE16-0001-02	Giovanni Marsicano
Fondation pour la Recherche Médicale	ARF20140129235	Luigi Bellocchio
Agence Nationale de la Recherche	ANR-10-LABX-0043	Giovanni Marsicano
Agence Nationale de la Recherche	ANR-18-CE14-0029-01	Giovanni Marsicano
Agence Nationale de la Recherche	ANR-19-CE14	Luigi Bellocchio

The funders had no role in study design, data collection and interpretation, or the decision to submit the work for publication.

Author contributions

Cristina Blázquez, Data curation, Software, Formal analysis, Validation, Investigation, Visualization, Methodology, Writing - review and editing; Andrea Ruiz-Calvo, Raquel Bajo-Grañeras, Data curation, Software, Formal analysis, Validation, Investigation, Visualization, Methodology; Jérôme M Baufreton, Conceptualization, Resources, Data curation, Software, Formal analysis, Validation, Investigation, Methodology; Eva Resel, Data curation, Investigation, Methodology, Project administration; Marjorie Varilh, Antonio C Pagano Zottola, Yamuna Mariani, Astrid Cannich, Data curation, Formal analysis, Validation, Investigation, Methodology; José A Rodríguez-Navarro, Conceptualization, Resources, Data curation, Formal analysis, Validation, Investigation, Methodology, Writing - review and editing; Giovanni Marsicano, Ismael Galve-Roperh, Conceptualization, Resources, Supervision, Funding acquisition, Methodology, Project administration, Writing - review and editing; Luigi Bellocchio, Conceptualization, Resources, Data curation, Software, Formal analysis, Supervision, Funding acquisition, Validation, Investigation, Visualization, Methodology, Project administration, Writing - review and editing; Manuel Guzmán, Conceptualization, Resources, Formal analysis, Supervision, Funding acquisition, Visualization, Methodology, Writing - original draft, Project administration, Writing - review and editing

Author ORCIDs

Jérôme M Baufreton https://orcid.org/0000-0002-2623-6375
Ismael Galve-Roperh http://orcid.org/0000-0003-3501-2434
Manuel Guzmán https://orcid.org/0000-0001-7475-118X

Ethics

Animal experimentation: All the experimental procedures were performed in accordance with the guidelines and with the approval of the Animal Welfare Committee of Universidad Complutense de Madrid and Comunidad de Madrid (PROEX 209/18), and in accordance with the directives of the European Commission (2010/63/EU). Adequate measures were taken to minimize pain and discomfort of the animals, as well as the number of animals used in the experiments, on the basis of the 3Rs (replacement, reduction and refinement) principle.

Decision letter and Author response

Decision letter https://doi.org/10.7554/eLife.56811.sa1
Author response https://doi.org/10.7554/eLife.56811.sa2

Additional files

Supplementary files

- Transparent reporting form

Data availability

All data generated or analysed during this study are included in the manuscript and supporting files. Source data files have been provided for Figures 1 through 6.

References

Alers S, Löffler AS, Wesselborg S, Stork B. 2012. Role of AMPK-mTOR-Ulk1/2 in the regulation of autophagy: cross talk, shortcuts, and feedbacks. *Molecular and Cellular Biology* **32**:2–11. DOI: https://doi.org/10.1128/MCB.06159-11, PMID: 22025673

Alpár A, Di Marzo V, Harkany T. 2016. At the tip of an iceberg: prenatal marijuana and its possible relation to neuropsychiatric outcome in the offspring. *Biological Psychiatry* **79**:e33–e45. DOI: https://doi.org/10.1016/j.biopsych.2015.09.009, PMID: 26549491

Araque A, Castillo PE, Manzoni OJ, Tonini R. 2017. Synaptic functions of endocannabinoid signaling in health and disease. *Neuropharmacology* **124**:13–24. DOI: https://doi.org/10.1016/j.neuropharm.2017.06.017, PMID: 28625718

Bagetta V, Picconi B, Marinucci S, Sgobio C, Pendolino V, Ghiglieri V, Fusco FR, Giampà C, Calabresi P. 2011. Dopamine-dependent long-term depression is expressed in striatal spiny neurons of both direct and indirect pathways: implications for parkinson's disease. *Journal of Neuroscience* **31**:12513–12522. DOI: https://doi.org/10.1523/JNEUROSCI.2236-11.2011, PMID: 21880913

Bellocchio L, Ruiz-Calvo A, Chiarlone A, Cabanas M, Resel E, Cazalets JR, Blázquez C, Cho YH, Galve-Roperh I, Guzmán M. 2016. Sustained Gq-Protein signaling disrupts striatal circuits via JNK. *Journal of Neuroscience* **36**:10611–10624. DOI: https://doi.org/10.1523/JNEUROSCI.1192-16.2016, PMID: 27733612

Birdsall V, Waites CL. 2019. Autophagy at the synapse. *Neuroscience Letters* **697**:24–28. DOI: https://doi.org/10.1016/j.neulet.2018.05.033, PMID: 29802916

Blázquez C, Chiarlone A, Sagredo O, Aguado T, Pazos MR, Resel E, Palazuelos J, Julien B, Salazar M, Börner C, Benito C, Carrasco C, Diez-Zaera M, Paoletti P, Díaz-Hernández M, Ruiz C, Sendtner M, Lucas JJ, de Yébenes JG, Marsicano G, et al. 2011. Loss of striatal type 1 cannabinoid receptors is a key pathogenic factor in Huntington's disease. *Brain* **134**:119–136. DOI: https://doi.org/10.1093/brain/awq278, PMID: 20929960

Blázquez C, Chiarlone A, Bellocchio L, Resel E, Pruunsild P, García-Rincón D, Sendtner M, Timmusk T, Lutz B, Galve-Roperh I, Guzmán M. 2015. The CB_1 cannabinoid receptor signals striatal neuroprotection via a PI3K/Akt/mTORC1/BDNF pathway. *Cell Death & Differentiation* **22**:1618–1629. DOI: https://doi.org/10.1038/cdd.2015.11, PMID: 25698444

Bockaert J, Marin P. 2015. mTOR in brain physiology and pathologies. *Physiological Reviews* **95**:1157–1187. DOI: https://doi.org/10.1152/physrev.00038.2014, PMID: 26269525

Castillo PE, Younts TJ, Chávez AE, Hashimotodani Y. 2012. Endocannabinoid signaling and synaptic function. *Neuron* **76**:70–81. DOI: https://doi.org/10.1016/j.neuron.2012.09.020, PMID: 23040807

Chiarlone A, Bellocchio L, Blázquez C, Resel E, Soria-Gómez E, Cannich A, Ferrero JJ, Sagredo O, Benito C, Romero J, Sánchez-Prieto J, Lutz B, Fernández-Ruiz J, Galve-Roperh I, Guzmán M. 2014. A restricted population of CB1 cannabinoid receptors with neuroprotective activity. *PNAS* **111**:8257–8262. DOI: https://doi.org/10.1073/pnas.1400988111, PMID: 24843137

Costa L, Amaral C, Teixeira N, Correia-da-Silva G, Fonseca BM. 2016. Cannabinoid-induced autophagy: protective or death role? *Prostaglandins & Other Lipid Mediators* **122**:54–63. DOI: https://doi.org/10.1016/j.prostaglandins.2015.12.006, PMID: 26732541

Covey DP, Mateo Y, Sulzer D, Cheer JF, Lovinger DM. 2017. Endocannabinoid modulation of dopamine neurotransmission. *Neuropharmacology* **124**:52–61. DOI: https://doi.org/10.1016/j.neuropharm.2017.04.033, PMID: 28450060

Davis MI, Crittenden JR, Feng AY, Kupferschmidt DA, Naydenov A, Stella N, Graybiel AM, Lovinger DM. 2018. The cannabinoid-1 receptor is abundantly expressed in striatal striosomes and striosome-dendron bouquets of the substantia nigra. *PLOS ONE* **13**:e0191436. DOI: https://doi.org/10.1371/journal.pone.0191436

DeBosch BJ, Heitmeier MR, Mayer AL, Higgins CB, Crowley JR, Kraft TE, Chi M, Newberry EP, Chen Z, Finck BN, Davidson NO, Yarasheski KE, Hruz PW, Moley KH. 2016. Trehalose inhibits solute carrier 2A (SLC2A) proteins to induce autophagy and prevent hepatic steatosis. *Science Signaling* **9**:ra21. DOI: https://doi.org/10.1126/scisignal.aac5472, PMID: 26905426

Dunlop EA, Tee AR. 2014. mTOR and autophagy: a dynamic relationship governed by nutrients and energy. *Seminars in Cell & Developmental Biology* **36**:121–129. DOI: https://doi.org/10.1016/j.semcdb.2014.08.006, PMID: 25158238

Emanuele E. 2014. Can trehalose prevent neurodegeneration? insights from experimental studies. *Current Drug Targets* **15**:551–557. DOI: https://doi.org/10.2174/1389450115666140225104705, PMID: 24568549

Englund A, Freeman TP, Murray RM, McGuire P. 2017. Can we make Cannabis safer? *The Lancet Psychiatry* **4**:643–648. DOI: https://doi.org/10.1016/S2215-0366(17)30075-5, PMID: 28259650

Gómez del Pulgar T, Velasco G, Guzmán M. 2000. The CB_1 cannabinoid receptor is coupled to the activation of protein kinase B/Akt. *Biochemical Journal* **347**:369–373. DOI: https://doi.org/10.1042/bj3470369, PMID: 10749665

Hara K, Maruki Y, Long X, Yoshino K, Oshiro N, Hidayat S, Tokunaga C, Avruch J, Yonezawa K. 2002. Raptor, a binding partner of target of rapamycin (TOR), Mediates TOR action. *Cell* **110**:177–189. DOI: https://doi.org/10.1016/S0092-8674(02)00833-4

Hiebel C, Kromm T, Stark M, Behl C. 2014. Cannabinoid receptor 1 modulates the autophagic flux independent of mTOR- and BECLIN1-complex. *Journal of Neurochemistry* **131**:484–497. DOI: https://doi.org/10.1111/jnc.12839, PMID: 25066892

Hiebel C, Behl C. 2015. The complex modulation of lysosomal degradation pathways by cannabinoid receptors 1 and 2. *Life Sciences* **138**:3–7. DOI: https://doi.org/10.1016/j.lfs.2015.03.020

Hill KP. 2015. Medical marijuana for treatment of chronic pain and other medical and psychiatric problems: a clinical review. *Jama* **313**:2474–2483. DOI: https://doi.org/10.1001/jama.2015.6199, PMID: 26103031

Hockly E, Woodman B, Mahal A, Lewis CM, Bates G. 2003. Standardization and statistical approaches to therapeutic trials in the R6/2 mouse. *Brain Research Bulletin* **61**:469–479. DOI: https://doi.org/10.1016/S0361-9230(03)00185-0, PMID: 13679245

Hosseinpour-Moghaddam K, Caraglia M, Sahebkar A. 2018. Autophagy induction by trehalose: molecular mechanisms and therapeutic impacts. *Journal of Cellular Physiology* **233**:6524–6543. DOI: https://doi.org/10.1002/jcp.26583, PMID: 29663416

Hudes G, Carducci M, Tomczak P, Dutcher J, Figlin R, Kapoor A, Staroslawska E, Sosman J, McDermott D, Bodrogi I, Kovacevic Z, Lesovoy V, Schmidt-Wolf IG, Barbarash O, Gokmen E, O'Toole T, Lustgarten S, Moore L, Motzer RJ, Global ARCC Trial. 2007. Temsirolimus, interferon alfa, or both for advanced renal-cell carcinoma. *New England Journal of Medicine* **356**:2271–2281. DOI: https://doi.org/10.1056/NEJMoa066838, PMID: 17538086

Janku F, Yap TA, Meric-Bernstam F. 2018. Targeting the PI3K pathway in Cancer: are we making headway? *Nature Reviews Clinical Oncology* **15**:273–291. DOI: https://doi.org/10.1038/nrclinonc.2018.28, PMID: 29508857

Katona I, Freund TF. 2008. Endocannabinoid signaling as a synaptic circuit breaker in neurological disease. *Nature Medicine* **14**:923–930. DOI: https://doi.org/10.1038/nm.f.1869, PMID: 18776886

Katsuragi Y, Ichimura Y, Komatsu M. 2015. p62/SQSTM1 functions as a signaling hub and an autophagy adaptor. *FEBS Journal* **282**:4672–4678. DOI: https://doi.org/10.1111/febs.13540, PMID: 26432171

Klugmann M, Symes CW, Leichtlein CB, Klaussner BK, Dunning J, Fong D, Young D, During MJ. 2005. AAV-mediated hippocampal expression of short and long homer 1 proteins differentially affect cognition and seizure activity in adult rats. *Molecular and Cellular Neuroscience* **28**:347–360. DOI: https://doi.org/10.1016/j.mcn.2004.10.002, PMID: 15691715

Koay LC, Rigby RJ, Wright KL. 2014. Cannabinoid-induced autophagy regulates suppressor of cytokine signaling-3 in intestinal epithelium. *American Journal of Physiology-Gastrointestinal and Liver Physiology* **307**:G140–G148. DOI: https://doi.org/10.1152/ajpgi.00317.2013, PMID: 24833710

Koketsu Y, Sakoda H, Fujishiro M, Kushiyama A, Fukushima Y, Ono H, Anai M, Kikuchi T, Fukuda T, Kamata H, Horike N, Uchijima Y, Kurihara H, Asano T. 2008. Hepatic overexpression of a dominant negative form of raptor enhances akt phosphorylation and restores insulin sensitivity in K/KAy mice. *American Journal of Physiology-Endocrinology and Metabolism* **294**:E719–E725. DOI: https://doi.org/10.1152/ajpendo.00253.2007, PMID: 18270303

Kreitzer AC. 2009. Physiology and pharmacology of striatal neurons. *Annual Review of Neuroscience* **32**:127–147. DOI: https://doi.org/10.1146/annurev.neuro.051508.135422, PMID: 19400717

Lebwohl D, Anak O, Sahmoud T, Klimovsky J, Elmroth I, Haas T, Posluszny J, Saletan S, Berg W. 2013. Development of Everolimus, a novel oral mTOR inhibitor, across a spectrum of diseases. *Annals of the New York Academy of Sciences* **1291**:14–32. DOI: https://doi.org/10.1111/nyas.12122, PMID: 23659703

Lee HJ, Yoon YS, Lee SJ. 2018. Mechanism of neuroprotection by trehalose: controversy surrounding autophagy induction. *Cell Death & Disease* **9**:712. DOI: https://doi.org/10.1038/s41419-018-0749-9, PMID: 29907758

Lemberger T, Parlato R, Dassesse D, Westphal M, Casanova E, Turiault M, Tronche F, Schiffmann SN, Schütz G. 2007. Expression of cre recombinase in dopaminoceptive neurons. *BMC Neuroscience* **8**:4. DOI: https://doi.org/10.1186/1471-2202-8-4, PMID: 17201924

Lipton JO, Sahin M. 2014. The neurology of mTOR. *Neuron* **84**:275–291. DOI: https://doi.org/10.1016/j.neuron.2014.09.034, PMID: 25374355

Lovinger DM. 2010. Neurotransmitter roles in synaptic modulation, plasticity and learning in the dorsal striatum. *Neuropharmacology* **58**:951–961. DOI: https://doi.org/10.1016/j.neuropharm.2010.01.008, PMID: 20096294

McMahon J, Huang X, Yang J, Komatsu M, Yue Z, Qian J, Zhu X, Huang Y. 2012. Impaired autophagy in neurons after disinhibition of mammalian target of rapamycin and its contribution to epileptogenesis. *Journal of Neuroscience* **32**:15704–15714. DOI: https://doi.org/10.1523/JNEUROSCI.2392-12.2012

Mechoulam R, Parker LA. 2013. The endocannabinoid system and the brain. *Annual Review of Psychology* **64**:21–47. DOI: https://doi.org/10.1146/annurev-psych-113011-143739, PMID: 22804774

Menzies FM, Fleming A, Caricasole A, Bento CF, Andrews SP, Ashkenazi A, Füllgrabe J, Jackson A, Jimenez Sanchez M, Karabiyik C, Licitra F, Lopez Ramirez A, Pavel M, Puri C, Renna M, Ricketts T, Schlotawa L, Vicinanza M, Won H, Zhu Y, et al. 2017. Autophagy and neurodegeneration: pathogenic mechanisms and therapeutic opportunities. *Neuron* **93**:1015–1034. DOI: https://doi.org/10.1016/j.neuron.2017.01.022, PMID: 28279350

Metna-Laurent M, Mondésir M, Grel A, Vallée M, Piazza PV. 2017. Cannabinoid-induced tetrad in mice. *Current Protocols in Neuroscience* **80**:1–10. DOI: https://doi.org/10.1002/cpns.31

Mizushima N, Yamamoto A, Matsui M, Yoshimori T, Ohsumi Y. 2004. In vivo analysis of autophagy in response to nutrient starvation using transgenic mice expressing a fluorescent autophagosome marker. *Molecular Biology of the Cell* **15**:1101–1111. DOI: https://doi.org/10.1091/mbc.e03-09-0704, PMID: 14699058

Mizushima N, Yoshimori T, Ohsumi Y. 2011. The role of atg proteins in autophagosome formation. *Annual Review of Cell and Developmental Biology* **27**:107–132. DOI: https://doi.org/10.1146/annurev-cellbio-092910-154005, PMID: 21801009

Monory K, Massa F, Egertová M, Eder M, Blaudzun H, Westenbroek R, Kelsch W, Jacob W, Marsch R, Ekker M, Long J, Rubenstein JL, Goebbels S, Nave KA, During M, Klugmann M, Wölfel B, Dodt HU, Zieglgänsberger W, Wotjak CT, et al. 2006. The endocannabinoid system controls key epileptogenic circuits in the Hippocampus. *Neuron* **51**:455–466. DOI: https://doi.org/10.1016/j.neuron.2006.07.006, PMID: 16908411

Monory K, Blaudzun H, Massa F, Kaiser N, Lemberger T, Schütz G, Wotjak CT, Lutz B, Marsicano G. 2007. Genetic dissection of behavioural and autonomic effects of Delta(9)-tetrahydrocannabinol in mice. *PLOS Biology* **5**:e269. DOI: https://doi.org/10.1371/journal.pbio.0050269, PMID: 17927447

Naydenov AV, Sepers MD, Swinney K, Raymond LA, Palmiter RD, Stella N. 2014. Genetic rescue of CB_1 receptors on medium spiny neurons prevents loss of excitatory striatal synapses but not motor impairment in HD mice. *Neurobiology of Disease* **71**:140–150. DOI: https://doi.org/10.1016/j.nbd.2014.08.009, PMID: 25134728

Ohsumi Y. 2014. Historical landmarks of autophagy research. *Cell Research* **24**:9–23. DOI: https://doi.org/10.1038/cr.2013.169, PMID: 24366340

Ozaita A, Puighermanal E, Maldonado R. 2007. Regulation of PI3K/Akt/GSK-3 pathway by cannabinoids in the brain. *Journal of Neurochemistry* **102**:1105–1114. DOI: https://doi.org/10.1111/j.1471-4159.2007.04642.x, PMID: 17484726

Pertwee RG, Howlett AC, Abood ME, Alexander SP, Di Marzo V, Elphick MR, Greasley PJ, Hansen HS, Kunos G, Mackie K, Mechoulam R, Ross RA. 2010. International union of basic and clinical pharmacology LXXIX cannabinoid receptors and their ligands: beyond CB_1 and CB_2. *Pharmacological Reviews* **62**:588–631. DOI: https://doi.org/10.1124/pr.110.003004, PMID: 21079038

Pertwee RG. 2012. Targeting the endocannabinoid system with cannabinoid receptor agonists: pharmacological strategies and therapeutic possibilities. *Philosophical Transactions of the Royal Society B: Biological Sciences* **367**:3353–3363. DOI: https://doi.org/10.1098/rstb.2011.0381

Piomelli D. 2003. The molecular logic of endocannabinoid signalling. *Nature Reviews Neuroscience* **4**:873–884. DOI: https://doi.org/10.1038/nrn1247, PMID: 14595399

Piyanova A, Albayram O, Rossi CA, Farwanah H, Michel K, Nicotera P, Sandhoff K, Bilkei-Gorzo A. 2013. Loss of CB_1 receptors leads to decreased cathepsin D levels and accelerated lipofuscin accumulation in the Hippocampus. *Mechanisms of Ageing and Development* **134**:391–399. DOI: https://doi.org/10.1016/j.mad.2013.08.001, PMID: 23954857

Puighermanal E, Marsicano G, Busquets-Garcia A, Lutz B, Maldonado R, Ozaita A. 2009. Cannabinoid modulation of hippocampal long-term memory is mediated by mTOR signaling. *Nature Neuroscience* **12**:1152–1158. DOI: https://doi.org/10.1038/nn.2369, PMID: 19648913

Puighermanal E, Busquets-Garcia A, Gomis-González M, Marsicano G, Maldonado R, Ozaita A. 2013. Dissociation of the pharmacological effects of THC by mTOR blockade. *Neuropsychopharmacology* **38**:1334–1343. DOI: https://doi.org/10.1038/npp.2013.31, PMID: 23358238

Richards AB, Krakowka S, Dexter LB, Schmid H, Wolterbeek AP, Waalkens-Berendsen DH, Shigoyuki A, Kurimoto M. 2002. Trehalose: a review of properties, history of use and human tolerance, and results of multiple safety studies. *Food and Chemical Toxicology* **40**:871–898. DOI: https://doi.org/10.1016/S0278-6915(02)00011-X, PMID: 12065209

Rodríguez-Navarro JA, Rodríguez L, Casarejos MJ, Solano RM, Gómez A, Perucho J, Cuervo AM, García de Yébenes J, Mena MA. 2010. Trehalose ameliorates dopaminergic and tau pathology in Parkin deleted/tau overexpressing mice through autophagy activation. *Neurobiology of Disease* **39**:423–438. DOI: https://doi.org/10.1016/j.nbd.2010.05.014, PMID: 20546895

Ruiz-Calvo A, Maroto IB, Bajo-Grañeras R, Chiarlone A, Gaudioso Á, Ferrero JJ, Resel E, Sánchez-Prieto J, Rodríguez-Navarro JA, Marsicano G, Galve-Roperh I, Bellocchio L, Guzmán M. 2018. Pathway-Specific control of striatal neuron vulnerability by corticostriatal cannabinoid CB1 receptors. *Cerebral Cortex* **28**:307–322. DOI: https://doi.org/10.1093/cercor/bhx285, PMID: 29121220

Salazar M, Carracedo A, Salanueva IJ, Hernández-Tiedra S, Lorente M, Egia A, Vázquez P, Blázquez C, Torres S, García S, Nowak J, Fimia GM, Piacentini M, Cecconi F, Pandolfi PP, González-Feria L, Iovanna JL, Guzmán M, Boya P, Velasco G. 2009. Cannabinoid action induces autophagy-mediated cell death through stimulation of ER stress in human glioma cells. *Journal of Clinical Investigation* **119**:1359–1372. DOI: https://doi.org/10.1172/JCI37948, PMID: 19425170

Sánchez-Martín P, Komatsu M. 2018. p62/SQSTM1 - steering the cell through health and disease. *Journal of Cell Science* **131**:jcs222836. DOI: https://doi.org/10.1242/jcs.222836, PMID: 30397181

Sarkar S, Davies JE, Huang Z, Tunnacliffe A, Rubinsztein DC. 2007. Trehalose, a novel mTOR-independent autophagy enhancer, accelerates the clearance of mutant huntingtin and alpha-synuclein. *Journal of Biological Chemistry* **282**:5641–5652. DOI: https://doi.org/10.1074/jbc.M609532200, PMID: 17182613

Sarkar C, Zhao Z, Aungst S, Sabirzhanov B, Faden AI, Lipinski MM. 2014. Impaired autophagy flux is associated with neuronal cell death after traumatic brain injury. *Autophagy* **10**:2208–2222. DOI: https://doi.org/10.4161/15548627.2014.981787, PMID: 25484084

Saxton RA, Sabatini DM. 2017. mTOR signaling in growth, metabolism, and disease. *Cell* **168**:960–976. DOI: https://doi.org/10.1016/j.cell.2017.02.004, PMID: 28283069

Shehata M, Matsumura H, Okubo-Suzuki R, Ohkawa N, Inokuchi K. 2012. Neuronal stimulation induces autophagy in hippocampal neurons that is involved in AMPA receptor degradation after chemical long-term depression. *Journal of Neuroscience* **32**:10413–10422. DOI: https://doi.org/10.1523/JNEUROSCI.4533-11.2012, PMID: 22836274

Suárez LM, Solís O, Caramés JM, Taravini IR, Solís JM, Murer MG, Moratalla R. 2014. L-DOPA treatment selectively restores spine density in dopamine receptor D2-expressing projection neurons in dyskinetic mice. *Biological Psychiatry* **75**:711–722. DOI: https://doi.org/10.1016/j.biopsych.2013.05.006, PMID: 23769604

Uchigashima M, Narushima M, Fukaya M, Katona I, Kano M, Watanabe M. 2007. Subcellular arrangement of molecules for 2-arachidonoyl-glycerol-mediated retrograde signaling and its physiological contribution to synaptic modulation in the striatum. *Journal of Neuroscience* **27**:3663–3676. DOI: https://doi.org/10.1523/JNEUROSCI.0448-07.2007, PMID: 17409230

Volkow ND, Baler RD, Compton WM, Weiss SR. 2014. Adverse health effects of marijuana use. *New England Journal of Medicine* **370**:2219–2227. DOI: https://doi.org/10.1056/NEJMra1402309, PMID: 24897085

Whiting PF, Wolff RF, Deshpande S, Di Nisio M, Duffy S, Hernandez AV, Keurentjes JC, Lang S, Misso K, Ryder S, Schmidlkofer S, Westwood M, Kleijnen J. 2015. Cannabinoids for medical use: a systematic review and Meta-analysis. *Jama* **313**:2456–2473. DOI: https://doi.org/10.1001/jama.2015.6358, PMID: 26103030

Wu YW, Kim JI, Tawfik VL, Lalchandani RR, Scherrer G, Ding JB. 2015. Input- and Cell-Type-Specific Endocannabinoid-Dependent LTD in the striatum. *Cell Reports* **10**:75–87. DOI: https://doi.org/10.1016/j.celrep.2014.12.005, PMID: 25543142

Yang DS, Stavrides P, Mohan PS, Kaushik S, Kumar A, Ohno M, Schmidt SD, Wesson D, Bandyopadhyay U, Jiang Y, Pawlik M, Peterhoff CM, Yang AJ, Wilson DA, St George-Hyslop P, Westaway D, Mathews PM, Levy E, Cuervo AM, Nixon RA. 2011. Reversal of autophagy dysfunction in the TgCRND8 mouse model of Alzheimer's disease ameliorates amyloid pathologies and memory deficits. *Brain* **134**:258–277. DOI: https://doi.org/10.1093/brain/awq341, PMID: 21186265

Zanardi E, Verzoni E, Grassi P, Necchi A, Giannatempo P, Raggi D, De Braud F, Procopio G. 2015. Clinical experience with temsirolimus in the treatment of advanced renal cell carcinoma. *Therapeutic Advances in Urology* **7**:152–161. DOI: https://doi.org/10.1177/1756287215574457, PMID: 26161146